Chem Catalysis

CellPress

Targeted Synthesis, Characterization, and Electrochemical Analysis of Transition Metal Oxide Catalysts for the Oxygen Evolution Reaction

Darius Hayes,[1,2] Shaun Alia,[2] Bryan Pivovar,[2] and Ryan Richards*[1,2]

[1]Department of Chemistry, Colorado School of Mines, Golden, CO 80401, USA

[2]National Renewable Energy Laboratory (NREL), Golden, CO 80401

*Correspondence: rrichard@mines.edu

SUMMARY

Hydrogen fuel can be produced through the electrochemical splitting of water, an energy intensive process which requires the use of electrocatalysts to make it more efficient. While current precious metal based electrocatalysts may be costly on a larger scale, transition metal oxide catalysts are more earth abundant and have shown promising activity. The development and improvement of highly active transition metal oxide electrocatalysts is thus an important area of study where different catalyst enhancement strategies are used to drive the field forward. Additionally, transition metal oxide catalyst come in various different structures with their own advantages; thus, this review is focused on investigating the continuing field of transition metal oxide electrocatalysts of different structures and innovative methods towards improving activity. Finally, new and promising paths forward in this field will be highlighted, particularly in the development of rock salt oxides for the water splitting system.

THE BIGGER PICTURE

By gaining increased understanding of the oxygen evolution reaction, current electrocatalyst design, and the structures of electrocatalysts used, more energy and cost efficient electrocatalysts will be developed for the water splitting system. As more idealized catalysts are developed, the water electrolysis method of developing hydrogen fuel will become a more tenable solution towards producing sustainable and renewable energy. The pursuit of sustainable energy sources has become more important than ever due to the growing impacts of climate change, thus a promising energy alternative to greenhouse gas emitting fossil fuels in the form of transition metal oxide based electrocatalysts is a valuable goal to investigate.

INTRODUCTION

As the damaging effects of climate change continue to impact the planet, the need for more efficient renewable energy sources has grown larger than ever. Hydrogen fuel is projected to be a valuable solution to the quest for renewable energy due to its power efficiency and reproducibility. 95% of current hydrogen is produced from fossil fuels via steam methane reforming and coal gasification processes – this product is referred to as "grey hydrogen"[1]. Due to its fossil fuel origins, the carbon emissions from grey hydrogen make it a non-ideal energy replacement. In contrast, "green hydrogen" is produced through water electrolysis, or electrochemically splitting water into hydrogen using energy from other renewable sources such as wind and solar energy. While this is a more ideal candidate for renewable energy, water electrolysis is a prohibitively high-cost technique that limits its practicality on a widespread scale. Water electrolysis is defined by two electrochemical reactions: the oxygen evolution reaction (OER) which occurs at the anode in an electrochemical cell, and the hydrogen evolution reaction (HER) which occurs at the cathode. According to figure 1A, the OER is a four-electron process in contrast to the HER's two electron process, making it slower and thus the main kinetic barrier that must be overcome to make electrolysis more efficient[2]. In this stead, electrocatalysts are used to catalyze both reactions.

The efficiency of electrocatalysts is measured through several key electrochemical parameters: overpotential, Tafel slope, turnover frequency (TOF), specific and mass activities, and stability[3]. Overpotential is the most commonly used parameter, defined as

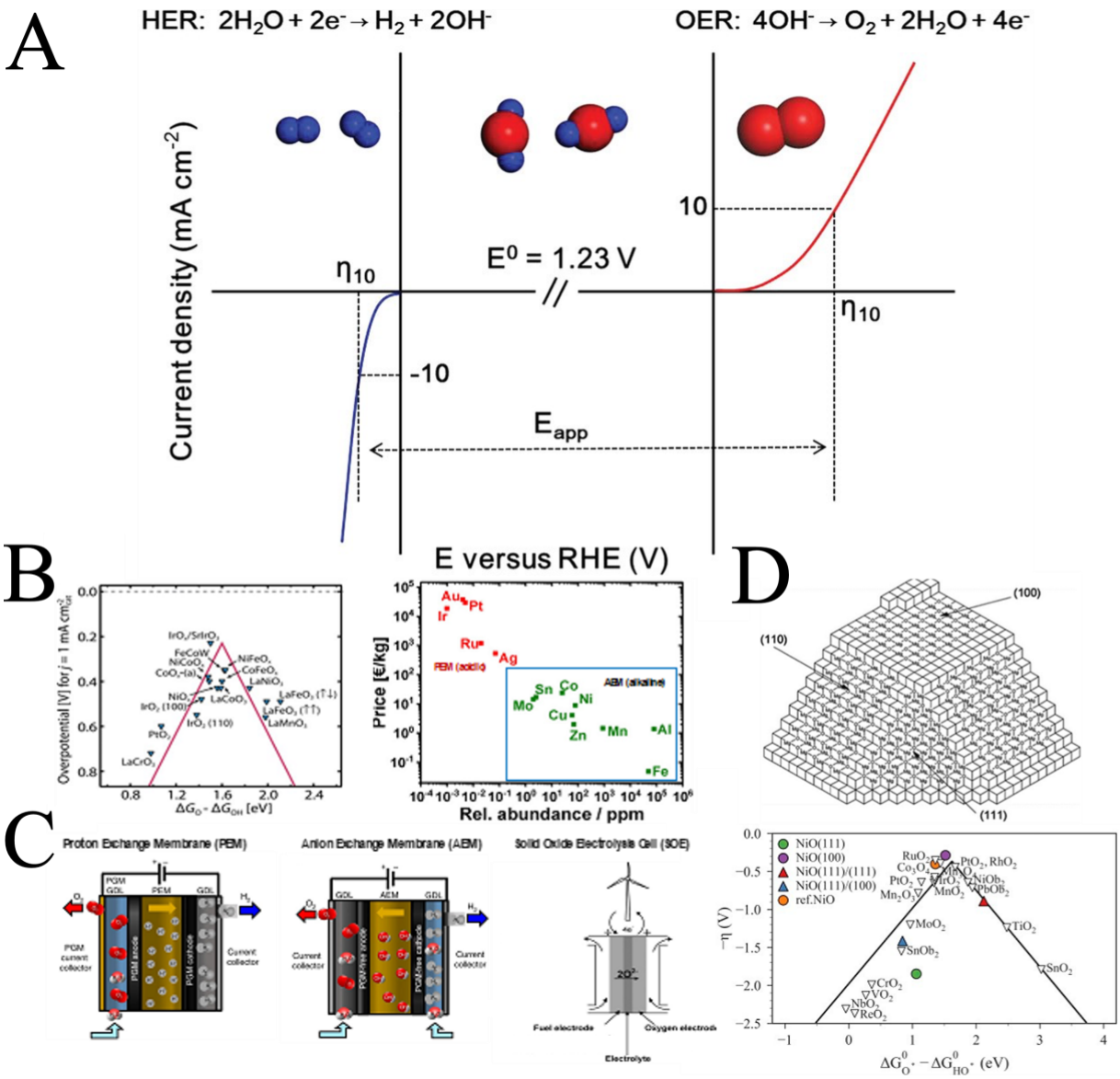

Figure 1: Current progress on green hydrogen production technology

(A) Polarization curves of the Oxygen Evolution Reaction (OER) and the Hydrogen Evolution Reaction (HER). Reprinted with permission from Yu et al.[3] Copyright 2021 John Wiley and Sons.

(B) Volcano plot of high performing OER catalysts and plot of earth abundance vs price for d-group metals. Reprinted with permission from Seh et al.[22] and Dresp and Stresser[5]. Copyright 2017 American Association for the Advancement of Science and 2018 John Wiley and Sons.

(C) Different types of electrolyzers. Reprinted with permission from Li et al[6] and Ebbesen et al.[7] Copyright 2020 Springer Nature and 2014 American Chemical Society.

(D) Different facets for rock salt metal oxide systems and catalytic activity of different nickel oxide facets. Reprinted with permission from Cadigan et al[11] and Sun et al[12]. Copyright 2011 Royal Society of Chemistry and 2019 PNAS.

the difference between the thermodynamic potential of the OER/HER and the experimental potential observed. Due to the nature of the difference, a smaller overpotential indicates less energy required for the reaction to occur and a better catalyst. The thermodynamic potential of the OER is commonly cited as 1.23V, thus catalysts with an overpotential around 400 mV or less are considered efficient candidates for electrolysis. Ideal

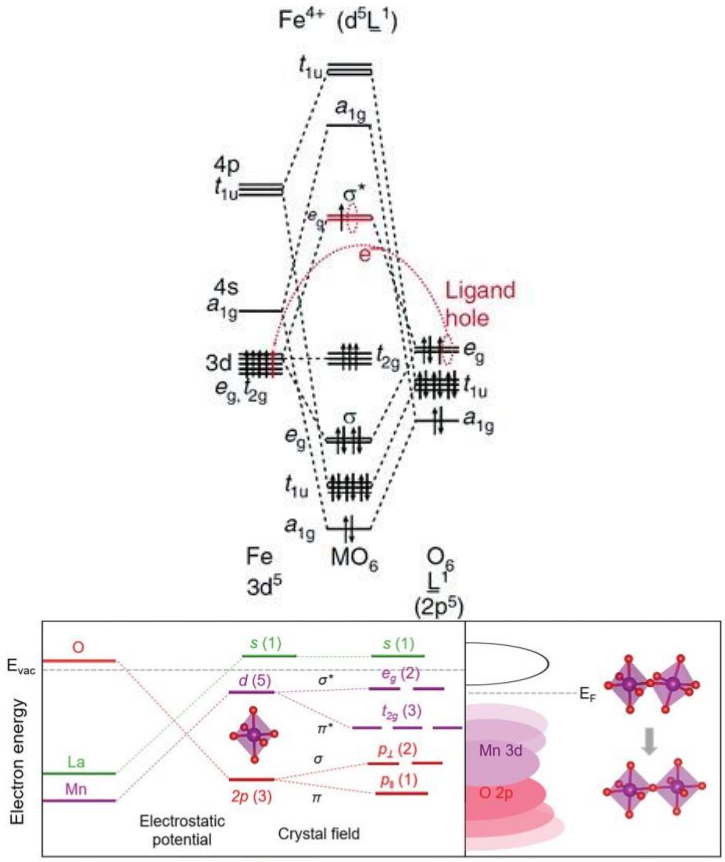

Figure 2: (Top) MO diagram of octahedral d orbitals (perovskite) and oxygen 2p orbitals. (Bottom) Difference in orbital energy levels due to electronic state splitting. Reprinted with permission from Li et al.[19] Copyright 2021 John Wiley and Sons.

electrocatalysts achieve higher current densities with lower overpotentials; the important parameter for OER catalysts is achieving a 10 mA cm^{-2} current density with the lowest overpotential possible[2]. The relationship between overpotential and current density is commonly depicted via Tafel plots, from which one may obtain the Tafel slope, another important electrochemical parameter. Tafel slopes describe how fast current increases versus the overpotential. Thus, a lower Tafel slope means a high current density is achieved through a lower overpotential, indicating better reaction kinetics[2]. Long-term stability is an additional important parameter for electrocatalysts. Different electrochemical tests are performed to monitor a catalyst's stability over several hours and continuous electrochemical cycles, such as chronopotentiometry and accelerated cyclic voltammetry (CV) respectively[3].

The current standard of electrocatalysts for water electrolyzers reaction are platinum group-based catalysts: examples include iridium oxide (IrO_x), the best performing catalyst for the OER, and ruthenium oxide (RuO_x), the best performing catalyst for the HER[4]. These precious metal catalysts are specifically used in the acidic environments of proton exchange membrane (PEM) electrolyzers. IrO_x displays an overpotential below 275 mV[2], thus providing an optimal balance of OER activity and stability for PEM systems. Once the focus shifts towards lower cost applications, however, the durability and lifetime of IrO_x systems becomes a concern. Additionally, as shown in figure 1B, the high cost and low availability of these precious metals increases the overall cost of the system, thus creating concerns on

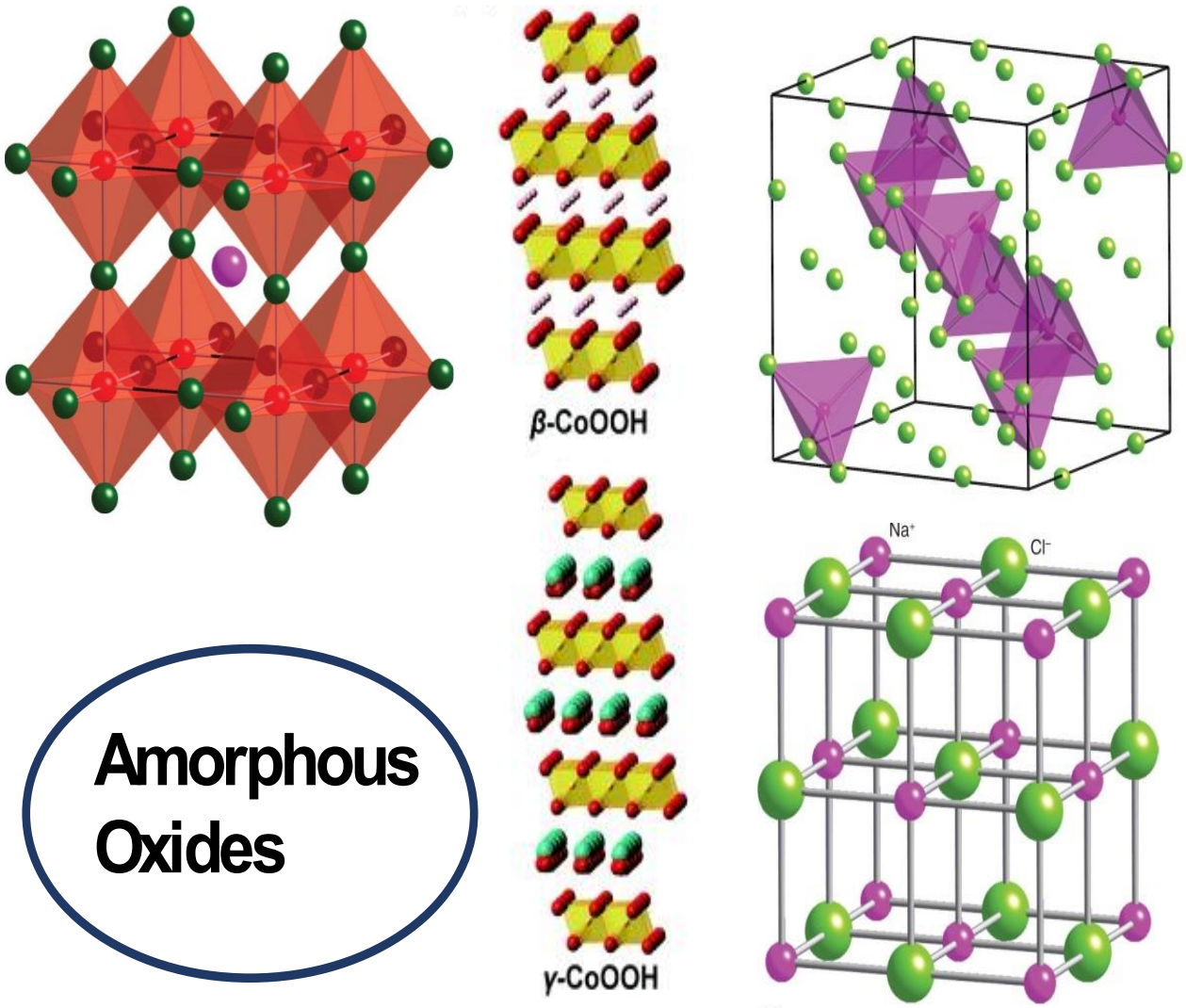

Figure 3: Crystal structures of different transition metal oxide families. Reprinted with permission from Suen et al.[2] and Weller.[45] Copyright 2017 Royal Society of Chemistry and 2018 Oxford Publishing Limited.

whether IrO_x systems can be implemented on a grid scale[4,5]. In order to lower the system costs for water electrolyzers, transition metal oxide electrocatalysts, such as manganese oxide, nickel oxide, and iron oxide, have been proposed as alternatives due to their earth abundance. These catalysts would be utilized in anion exchange membrane (AEM) electrolyzers, which operate in an alkaline environment instead of the acidic environment of PEM systems[6]. These different electrolyzer systems, as well as solid oxide electrolysis cells[7], are displayed in figure 1C.

The activity of a catalyst may be improved through two (non-mutually exclusive)means: increasing the number of active sites and increasing intrinsic activity. Improving surface area and activity impacts the specific and mass activities, two vital parameters to catalyst activity. Normalization of the catalyst's current density to either the electrochemical surface area (ECSA) or the Brunauer-Emmett-Teller (BET) surface area provides the specific activity of a catalyst, specifically providing an idea of the intrinsic activity of the catalyst's active sites. Additionally, normalizing the current to the catalyst's loading mass provides mass activity [8], which is affected by the catalyst's active surface area.

In the process of designing efficient catalysts, characterization of the catalysts is vital for understanding how to improve their activity. The most commonly used techniques for OER catalyst characterization are transmission electron microscopy (TEM), X-ray diffraction (XRD), and X-ray photoelectron spectroscopy (XPS). TEM is usually used in high resolution (HRTEM) to provide information on catalyst shape, morphology, and surface faceting. Additionally, energy-dispersive x-ray spectroscopy (EDS) is used to determine the location of each chemical element in the catalyst system; this is useful for compositional analysis. XRD is commonly used to determine the crystalline structure and identity of the catalyst, alongside learning which crystallographic phases are present. XPS is a powerful tool for observing the chemical species and oxidation states present in the system; this is useful for learning which elements and ions are most beneficial for the OER. Other characterization techniques can be used for further characterization knowledge, such as physisorption and chemisorption analysis. Physisorption analysis in particular is useful for determining the catalyst surface area which is vital for understanding mass activity.

Transition metal oxide catalysts may be synthesized into a breadth of different structures, such as layered double hydroxides (LDH), spinels, and rock salts. Of these transition metal electrocatalysts, nickel oxides have shown some of the highest catalytic activity, comparable to that of IrO_x catalysts[9]. Nickel oxide compounds of various structures, including layered double hydroxides (LDHs) and spinels, have all shown promising overpotential values. Further improvement in overpotentials can be achieved through doping nickel oxides with additional transition metals; specifically, FeNiO LDHs, spinels, and rock salts are among the best performing electrocatalysts[10]. Theoretical studies have shown that altering the surface morphology of nickel oxide systems, primarily the surface facets, should improve their catalytic activity to become on of the most ideal OER catalysts. As shown in figure 1D, NiO in the (100) facet has among the highest theoretical catalytic activity in comparison to the (111) facet, which is the more common and stable product of wet chemical NiO syntheses[11, 12]. With this prediction in mind, further research must be done to study the impact of morphological effects on nickel oxide, and by extension electrocatalysts for the OER. Due to their relative morphological flexibility, rock salt compounds are a good candidate to study these effects on OER activity. This review will investigate the synthesis and characterization of transition metal electrocatalysts with a focus on the different approaches to improve their catalytic activity for the OER, and how these techniques and the knowledge gained from them can be combined to further the understanding and development of this technology for renewable energy.

Oxygen Evolution Reaction Mechanism and Electrochemical Characterization

The first step to successfully designing efficient electrocatalysts is understanding the oxygen evolution reaction via deciphering the reaction mechanism. While much research has been conducted on the OER, there is still much discussion and debate on the exact mechanism. As such, there are three commonly discussed OER mechanisms that will be compared in this section: the Adsorbent Evolution Mechanism (AEM), the Lattice Oxygen Mechanism (LOM), and the Oxide Path Mechanism (OPM)[13].
While the proposed OER mechanisms have specific differences in their steps, one important common factor is these steps all take place on the metal surface (M). After each reaction step, a different intermediate is formed in the form of M-O*, M-OH*, and M-OOH* intermediates[14]. The overall reaction energy is then comprised of the adsorption energy difference between the different intermediates, primarily the ΔG difference between M-O and M-OH intermediates. Calculating the intermediate binding energy difference is one of the main descriptors of catalytic activity, usually depicted in reaction free energy diagrams referred to as "volcano plots"[11]. The relationship between M-O and M-OH intermediates affects the overall reaction rate depending on how strongly oxygen binds to the surface: strong binding of oxygen to the catalyst's surface prevents MOOH formation, in contrast to weak oxygen binding preventing MO formation[15]. Previous theoretical studies have established that ideal catalytic activity correlates to a $\Delta G_{O\text{-}OH}$ close to zero so that oxygen binds neither too strongly nor weakly; this concept is referred to as the Sabatier Principle[16]. The binding energy of intermediates can be further influenced through additional factors such as different adsorbed species, solvent interactions, and surface vacancies. One major factor that affects intermediate binding energy is the number of e_g electrons present, where

studies have shown e_g values closer to unity (one) improve OER activity significantly[17]. As is shown in Figure 2, this relationship is due to improved overlap between the metal d orbitals (specifically in the octahedral configuration) and oxygen 2p orbitals along the z-axis[18,19] Studies done on transition metal perovskite oxide systems in question have shown that when transition metal oxide ions have the e_g^1 configuration, there is increased covalency between the transition metal 3d orbitals and the oxygen 2p orbitals. This is shown in the bottom part of figure 2, where electronic state splitting in the octahedral geometry leads to better orbital overlap. The hydrogen bond in hydroxyl groups has also been shown to stabilize M-OH and M-OOH intermediates in contrast to M-O intermediates.

The most common and established OER mechanism is the adsorbent evolution mechanism (AEM), shown in Equation 1. The AEM consists of four consecutive proton-coupled electron transfer steps on the M site that yield O_2[10].

$$(1)\ M + OH^- \rightarrow MOH + e^-$$
$$(2)\ MOH + OH^- \rightarrow MO + H_2O + e^-$$
$$(3)\ MO + OH^- \rightarrow MOOH + e^-$$
$$(4)\ MOOH + OH \rightarrow H_2O + O_2 + e^-$$

Equation 1: Adsorbent Evolution Mechanism

The electronic structure of the metal oxide band has a large impact on which mechanism occurs. When the metal d-band atoms are located above the oxygen p-band atoms in the metal oxide's electronic structure, the metal atoms then play the role of adsorption center and drive the process towards the AEM. In contrast, when the oxygen p-band atoms are higher, electron transfer is observed from oxygen p-band to metal d-band. This electron transfer leads to ligand holes and the release of oxygen forming oxygen vacancies[13]. The increased metal oxygen covalency thus pushes the process towards the lattice oxygen mechanism (LOM) through the increased oxygen adsorption energy. The mechanism of the LOM is less defined due to not being as extensively studied as the AEM; one proposed mechanism for the LOM is given in Equation 2[13], where V_o represents the oxygen vacancy.

$$(1)\ MO + H_2O \rightarrow MOOH + H^- + e^-$$
$$(2)\ MOOH \rightarrow MV_O + O_2 + H^- + e^-$$
$$(3)\ MV_O + H_2O \rightarrow MOH + H^- + e^-$$
$$(4)\ MOH \rightarrow MO + H^- + e^-$$

Equation 2: Lattice Oxygen Mechanism

The lattice oxygen mechanism primarily relies on lattice oxygen activation and O-O coupling in the OER, thus creating oxygen vacancies that can separate metal species and the catalyst surface to cause catalyst degradation. To avoid this degradation, another mechanism involving O-O coupling can be used: the oxide path mechanism (OPM), shown in Equation 2. First cited in 1956, the oxide path mechanism involves only MO and MOH intermediates:

$$(1)\ M + OH^- \rightarrow MOH + e^-$$
$$(2)\ 2M - OH \rightarrow MO + H_2O + M$$
$$(3)\ 2MO \rightarrow 2M + O_2$$

Equation 3: Oxide Path Mechanism

By using direct O-O coupling without oxygen vacancies degrading the catalyst, the OPM can affect the scaling relationship between AEM and LOM. This is due to the OPM providing more MO and MOH intermediates without an increase in MOOH intermediates; however, stricter active site configurations are required for the OPM than the other two mechanisms[13]. An example of this configuration is the $CaCU_3Fe_4O_{12}$ perovskite oxide catalysts that was synthesized for OER, where the incorporation of Fe^{4+} and Cu^{2+} lead to the oxygen-oxygen bonds being bent and shortened lower than usual, thus allowing direct O-O bond formation[17].

With an understanding of the OER mechanism, electrochemical characterization techniques such as cyclic voltammetry (CV), linear sweep voltammetry (LSV), and electrochemical impedance spectroscopy (EIS) can be used as a primary method of measuring electrocatalyst activity for the OER. Cyclic voltammetry is one of the most commonly used electrochemical techniques for investigating redox processes, studying chemical reactions involving electron transfer, and measuring current between electrodes[20,21]. CV experiments are typically conducted with the three-electrode set-up of the working electrode (WE), counter electrode (CE), and reference electrode (RE). In this set up, the WE serves as the redox site, the CE as an electron source, and the RE as a stable potential source that is used to calculate the WE potential[21]. These electrodes are placed in the electrolyte solution, an ionic conductive solution made from a diluted dissolved inorganic salt (such as sodium or potassium hydroxide). The electrode setup is connected to a potentiostat that controls the WE potential which produces current-potential polarization curves known as voltammograms; here the current is measured between the WE and CE versus the potential measured between the WE and RE. Important parameters in the voltammograms are the peak potentials, the potentials where the current maximum is reached during either the positive (peak anodic potential E_{pa}) or negative (peak cathodic potential E_{ca}), the current calculated between the cathodic and anodic currents against the resting current (i_{pc} and i_{pa}), and the scan rate of the electrochemical measurement. Similar to the CV technique is linear sweep voltammetry (LSV), which involves the same set-up and parameters as CV but involving only one sweep between the upper and lower potential limits instead of cycling in both directions like the CV.

Electrochemical Impedance Spectroscopy (EIS) is another popular electrochemical technique for finding physical properties of the electrode surface, particularly information about resistances and charge transfer kinetics. The frequency at which EIS measurements are taken ranges from 100 kHZ to 100 mHZ, and the information gained from the measurement varies with frequency. In high frequency ranges, the faraday process is not observed so the resistance is independent of applied potential and thus reflects the resistances of the substrate and catalyst material; however, medium and low frequency ranges can be used to infer information on the charge transport and charge transfer resistance (R_{ct}) respectively[3]. R_{ct} analysis is typically done with Nyquist plots that show impedance as a semi-circle.

Catalyst Activity Enhancement Strategies

In the pursuit of improving electrocatalyst activity, it is commonly understood that there are two main approaches to accomplishing this goal: improving the number of active sites present on the catalyst surface and improving the intrinsic activity of said active sites[22]. The number of catalyst active sites is known to correspond with catalyst surface area therefore it is believed that increasing active sites can be achieved by similar means (ie. inducing

Defect Engineering	Surface Reconstruction	Crystal Engineering	Interface Engineering
Positive: • Oxygen and anion vacancies improve intermediate adsorption energy	Positive: • Reconstruction increases amount of highly active sites	Positive: • Increased number of active sites and intrinsic activity by facet	Positive: • Improve surface area, charge transfer, and electronic structure modulation
Challenges: • Techniques tend to be destructive and/or corrosive	Challenges: • Reconstruction is irreversible on some catalysts hinders cycling ability	Challenges: • Thermodynamically difficult to synthesize some facets	Challenges: • Long, energy intensive synthetic routes

Table 1: Comparison of different catalyst enhancement strategies.

porosity, forming thin films, etc.); however, the consensus among theoretical studies is that increasing the intrinsic activity will have the most substantial effect on improving catalyst OER activity[23].

With these two enhancement pathways in mind, extensive work in both synthesis and theoretical calculations has been done in the field of oxygen evolution catalysis to determine multiple efficient strategies to achieve the targeted OER improvements.

Cation and Anion Vacancy Engineering

Utilizing defects in both anions (oxygen vacancies) and cations (metal vacancies) is an established method of improving activity by altering the electronic structure of said catalysts. Oxygen vacancies are the main representative of anion defects (usually depicted as V_o) and are known to improve reaction kinetics by promoting intermediate adsorption via lowering the surface activation energy. The effect of oxygen vacancies has been studied in a myriad of different transition metal catalysts. One example is the reduced spinel Co_3O_4 nanowires[24] shown in figure 4A, where the oxygen vacancy filled nanowires showed over seven times the performance of pristine Co_3O_4 and slightly higher performance than IrO_2, the standard OER catalyst. DFT calculations were done on these reduced nanowires to determine that the oxygen vacancies caused electron delocalization and increased Co_3O_4 conductivity, thus inciting increased performance. Oxygen vacancy tuning can be done on further transition metal catalysts; ultra-small (2.1 nm) NiO nanoparticles with rich oxygen vacancies were produced through laser synthesis that showed an overpotential above bulk NiO and similar to RuO[25]. This increased performance was attributed to faster reaction kinetics through oxygen vacancies and increased active sites exposed due to the small size.

On the other end of defect engineering are cation defects, which commonly come in the form of metal vacancies. Cation vacancies have been shown to be a useful method of OER development due to their ability to increase catalyst stability and improve intermediate binding energy as demonstrated in the synthesis of cation vacancy engineered NiFe-LDHs[26]. NiFe-LDHs are some of the most promising alkaline OER candidates, however they are regularly plagued by poor stability; controlled synthesis was used to produce $M^{2+/3}$ vacancies in the NiFe-LDH basal plane to improve catalyst stability through strengthening M-O bonding and preventing metal dissolution through lattice distortion. Additionally, metal vacancies were shown to further improve the OER activity of NiFe-LDHs by pushing γ-(NiFe)OOH active sites to evolution and thus improving OER intermediate binding energy.

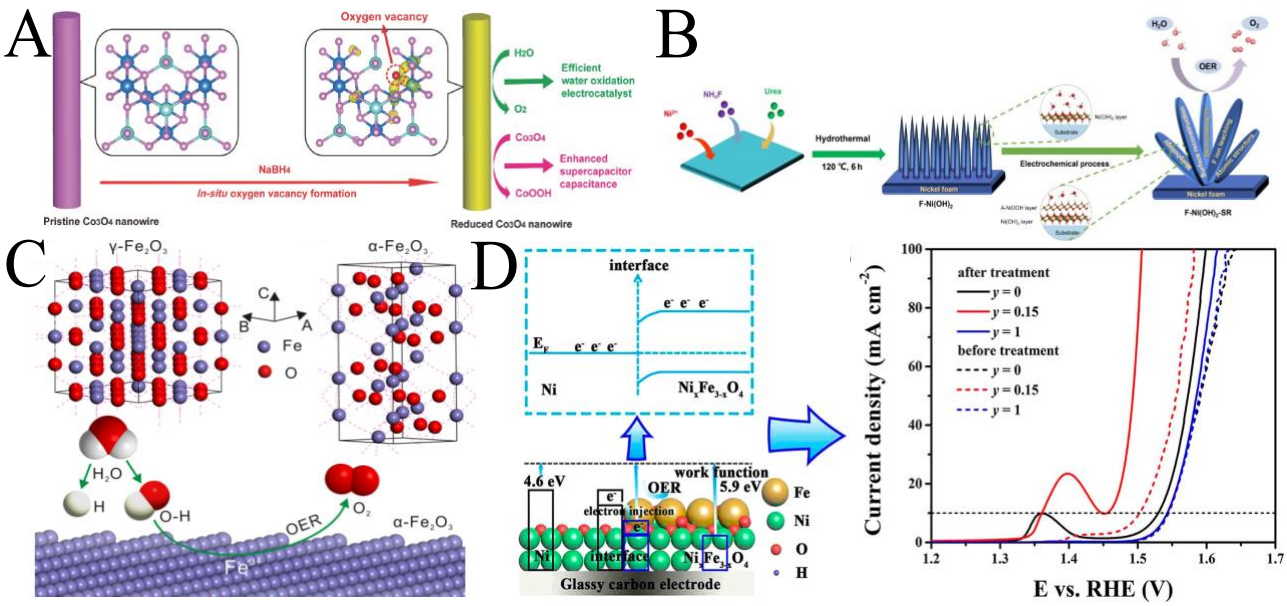

Figure 4: Examples of the highlighted catalyst enhancement strategies.

(A) Introduction of oxygen vacancies into Co_3O_4 spinel nanowires. Reprinted with permission from Zheng et al.[24] Copyright 2014 John Wiley and Sons.

(B) Electrochemical incorporation of F anions into $Ni(OH)_2$ structures to induce surface reconstruction. Reprinted with permission from Kang et al.[27] Copyright 2021 Springer Nature.

(C) Fe_2O_3 materials synthesized in different phases (α and γ). Reprinted with permission from Xu et al.[30] Copyright 2020 Elsevier.

(D) Mott-Schottky effect used to induce increased electron transfer on $Ni_xFe_{3-x}O_4$/Ni semi-conductor/metal interface. Reprinted with permission from Huang et al.[41] Copyright 2018 American Chemical Society.

Vacancy engineering has been shown to be effective at improving OER catalytic activity through increasing the number of active sites on catalyst as was seen with improved peak current density of the reduced mesoporous Co_3O_4 nanowires[24]. By using vacancies to provide additional active sites, one of the main pathways towards improving electrocatalyst activity is achieved.

Altering Surface Reconstruction Rates

Presently, one of the most important strategies for improving catalyst OER performance is the usage of surface reconstruction to provide more ideal active species for the reaction. It has been discovered through multiple mechanistic studies that structural reconstruction will occur on the catalyst surface during the electro-oxidation process, thus forming a new active species. In particular, transition metal oxyhydroxides (such as FeOOH, NiOOH, and CoOOH) have been shown to be the most common active species post surface oxidation. With this in mind, it is important to elucidate a way to practically control surface reconstruction during the OER. One such way to achieve this goal is through the use of highly electronegative anions into the catalyst structure. F anions were incorporated into $Ni(OH)_2$ structures as a method to improve targeted regulation of surface structure[27]. In this study, F-$Ni(OH)_2$ materials were synthesized on nickel foam using a hydrothermal method, then put the materials through cyclic voltammetry treatments (in intervals of 50, 100, 150, 200, and 250 cycles) to observe the difference in activity through further surface reconstructions post-oxidation (figure 4B). They discovered that F-$Ni(OH)_2$ after 200 cycles (F-$Ni(OH)_2$-SR-200) showed substantial OER activity at an overpotential of 287 mV at 10 $mA \cdot cm^{-2}$, which was attributed to the strongly electronegative F anions leaching onto the surface layer during the cycling reactions. This led to multiple effects such as a space-charge effect that affects electron charge densities, and improved ion adsorption and charge-transfer on the catalyst.

The impact of heteroatom doping is also transparent in other TM catalyst structures, as is shown by doping S into NiFe LDHs[28] with a shown overpotential of 259 mV at 100 mA·cm^{-2}. Computational studies done in this paper suggest that S-Ni_xFe_yOOH formed as a result of reconstruction optimizes the adsorption energy of intermediates and improves activity; further characterization such as XRD and XANES was used to determine that S substituted lattice O to dissuade belief that SO_x ligands were formed instead. From these studies, it is evident that element doping will prove to be a powerful tool in the effort of improving catalyst activity.

Additional ways to impart fast surface reconstruction is strict control of initial structure and morphology of the transition metal catalyst. This was displayed via the difference between amorphous NiFeMoO catalysts with its crystalline counterpart to highlight this strategy[29]. The amorphous NiFeMoO catalysts recorded an overpotential of 280 mV at 10 mA·cm^{-2}, which is a marked improvement to crystalline NiFeMoO at 358 mV, Ir/C at 440 mV, and RuO_2 at 480 mV. This efficient overpotential was attributed to the amorphous features granting the catalyst greater cation diffusion capability than its cation counterpart, thus lowering the formation energy for oxygen vacancies (which were established as a boon for OER activity in the previous section).

Surface reconstruction is a powerful tool for improving the number of active sites on a catalyst surface. This was shown with the F-$Ni(OH)_2$ catalysts[27], where surface reconstruction lead to more NiOOH, the true active site, present on the surface. Being a consistent way t0 increase active sites on the electrocatalyst surface makes surface reconstruction a valuable strategy for OER studies.

Effects of Crystal Phases and Facets

One approach to affect catalyst activity common amongst the different structures of transition metal catalysts is through crystal engineering. In this world of crystal engineering, the two main pathways toward activity improvement come in the form of crystal phase engineering and crystal facet engineering.

Crystal phase engineering is most promisingly displayed in the studies of the different phases of Fe_2O_3, commonly agreed to be one of the most promising OER candidates. Fe_2O_3 are known to come in the natural forms of α-Fe_2O_3 and γ-Fe_2O_3 (as shown in figure 4C), where the difference in OER activity was investigated in a study involving yolk-shell microspheres[30]. Here, it was demonstrated that α-Fe_2O_3 (275 mV) showed an improved overpotential at 10 mA·cm^{-2} compared to γ-Fe_2O_3 (340 mV), where XPS spectra survey was used to attribute this stronger activity with the idea that α-Fe_2O_3 has more easily exposed Fe active sites than γ-Fe_2O_3; this supports previously findings that Fe cations regularly enhance OER activity through Fe serving as one of the main active sites[31]. Interestingly, this study was taken further by Hu et al. who investigated the impact of mixed-phase FeOOH systems[32]. In the comparison between single phase (α, β, and δ) and multi-phase (α/β, α/δ, and β/δ) FeOOH systems, β/δ-FeOOH proved the most efficient. To understand the difference, the partial density states of this system was calculated and revealed that thanks to $t_{2g}^6e_g^1$ electronic configuration of the Fe 3d orbitals, a Jahn-Teller effect was present to induce lattice distortion. As such, it is once again displayed that the presence of oxygen vacancies and electronic structure optimization plays a large role in OER activity. A similar crystal phase study was completed by Meng et al. on MnO_2, where it was displayed that α-MnO_2 shows the best overpotential amongst different MnO_2 phases (albeit worse than Ni and Fe counterparts at 490 mV at 10 mA·cm^{-2}), which was attributed to the accessibility of μ_2-oxo-O(H) active sites in its structure[33].

Controlled faceting has shown promise as a method towards affecting OER activity. It is known that inorganic catalysts are made up of crystals that display anisotropic features that will vary based on the facets present. Previous studies have then confirmed that certain exposed facets possess more active sites that can improve reactivity thanks to improved mass activity[25]. As such, understanding how to control catalyst crystal morphology and select the most highly active crystal plane is an ideal strategy for enhancing activity. One can notice the effect of crystal plane selection through observing the higher surface energy of

high-index facets (as a feature of their high density of low-coordinated atoms on their steps and kinks) [34]; this is further reflected in their enhanced catalytic activity as is displayed in the study of high index Co_3O_4, where Co_3O_4 in the [112] facet filled with oxygen vacancies showed a favorable overpotential of 318 mV at 10 mA·cm^{-2} [35]. Unfortunately, a regular problem towards the use of high-index facets is their tendency to diminish in normal synthetic conditions as high surface energy facets are associated with high supersaturation solutions, which are known to be relatively less stable[36]. One way to counter this phenomenon is through the use of the selective etching strategy to target which planes will be preserved and which will be dissolved. An unconventional version of this strategy was displayed when acid was used to yield the unconventional [012] facet in α-Fe_2O_3 for the OER that displayed a low overpotential of 317 at 10 mA·cm^{-2} [37]. DFT calculations were used to contrast the [012] facets with the [104] facet (which showed excessively weak intermediate adsorption energies] and the [110] facet (displaying excessively strong intermediate adsorption energies on the other end). This work displays the promising efficiency of crystal facet engineering in the pursuit of improved OER performance.

This strategy is used for transition metal catalysts of various structures such as LDHs, where the layered structure is capable of providing more active sites. The difference between the normally low activity [003] plane and more active [012] edge was probed in a display of crystal facet engineering in LDHs[38]. Here, the [012] edge showed a far improved overpotential of 250 mV at 100 mA·cm^{-2} (with the current density nearly five times higher than the [003] plane at the same overpotential); this was attributed to the improved oxygen coordination at the Fe sites. Through these studies, the value of crystal facet engineering becomes readily apparent, thus making it one of leading strategies for improving OER performance.

Crystal engineering is an important strategy for improving catalyst activity due to its ability to increase the number of active sites available through phase engineering, such as in the α-Fe_2O_3 study[32], alongside improving the intrinsic activity of the catalyst through facet. The improvement in catalyst intrinsic activity was noted with the substantially higher TOF value shown in α-Fe_2O_3 in the [012] facet[37]. The bifunctional nature of crystal engineering makes it a valuable toolset to consider for OER catalysis.

Interface Engineering/Dopant and Compositional Effects

Engineering the heterogeneous interface of transition metal catalysts is another approach to improving the intrinsic activity of the active site and thus improving OER kinetics. Through interface engineering, one is able to improve the active site density and further regulate the catalyst's electronic structure. Examples of interface engineering include optimization at the interface between the metal oxide catalyst and support, interaction between the catalyst and additional metals doped into its structure, and between two metal oxides within the catalyst system.

The core principle that drives interface engineering is the synergistic effect, where it is observed that a multi-component material, in this case a metal oxide catalyst on a support, will provide more opportunities for ideal reactant or intermediate binding. This effect subsequently leads to better OER activity than non-surface engineered catalysts. Previous studies have shown that the heterogeneous interface in particular can be largely improved through synergistic effects that increase the catalyst's electron transfer ability. One example is the Mott-Schottky effect that occurs at the interface between a metal and semiconductor. This interface effect is efficient at directing electron densities towards better reaction kinetics due to electrons being able to flow from the component with a lower work function (the minimum energy required to remove an electron from inside a metal to a position just outside of its surface [39]) to the higher work function component until equilibrium is achieved[40].

This effect can be seen in transition metal electrocatalysis in the study of $Ni_xFe_{3-x}O_4$/Ni metal nanocomposites[41]. Spinel oxides, such as $Ni_xFe_{3-x}O_4$, are known to have very limited electrical conductivity due to their semi-conductor nature, thus Huang et al investigated the impacts of metal and oxide interaction through coupling with Ni metal nanoparticles to form

hybrid nanostructures via solvothermal synthesis, displayed in figure 4D. These nanostructures showed excellent OER performance with an overpotential of 225 mV at 10 mA·cm^{-2}, some of the highest activity for spinel oxide electrocatalysts. This study also reiterates the impact of Fe in Ni compounds by probing structures with varying levels of Fe incorporation through a calculated y-value equal to Fe/(Fe + Ni); from this equation, they tested a range of values from y= 0 to y=1.0, where they found that the ideal Fe ratio to be at y=0.15. This is similar to previous Fe incorporation studies that have shown that adding too little or too much Fe provides suboptimal OER activity[18]. The overall improved electrocatalysis of this semiconductor system was explained by observing the lower work function of Ni metal compared to $Ni_xFe_{3-x}O_4$ (4.60 eV to 5.9 eV), which in turn allows electrons to more easily travel from through the catalyst interface until equilibrium between the work functions are achieved. The Mott Schottky effect can be observed amongst other transition metal electrocatalysts such as the Co/Co_3O_4 nanoparticles encapsulated by N-doped carbon nanotubes for OER applications in zinc-air batteries[42]. The produced hetero-nanoparticle samples displayed an impressive overpotential of 275 mV at 10 mA·cm^{-2}; similar to the previously mentioned iron and nickel-based samples, these difference in work function between the metallic Co and semi-conductor Co_3O_4 induced electron transfer across the heterointerface and thus lowering the reaction energy barriers. Here, one can also observe the usage of supports in interface engineering where the N-doped carbon nanotubes support improved mass diffusion and electron transfer as well as improving structural and electrochemical stability.

In addition to the impacts of synergistic effects, interface engineering can be used to modulate the electronic surfaces present at catalyst interfaces; in conjunction with the previously discussed defect engineering, altering the catalyst electronic structure is a reliable strategy to improve electron-transfer kinetics and active site density. A high performance Co_3O_4 and NiFe-LDH core-shell catalyst with a nickel foam (NF) support was synthesized to investigate the effects of hetero-interface engineering[43]. OER overpotentials were tested over a current density range of 10 to 500 mA·cm^{-2}, where NiFe-60/Co_3O_4@NF, the sample in which NiFe was electrodeposited onto Co_3O_4@NF for 60 seconds, displayed an overpotential of 190 mV at 10 mA·cm^{-2} alongside impressive long-term stability. The NiFe-LDH forms a hetero-interface composed of an amorphous area rich with uncoordinated metal sites and a high stability crystalline area. The interaction between the different metal species through the heterointerface optimizes the catalyst's electronic structure, thus leading to improved catalytic activity.

Similar to the defect engineering strategy on the catalyst, defects may also be introduced into catalyst interfaces to introduce oxygen vacancies, induce the synergistic effect, and thus improve electrocatalytic activity. A defect incorporated heterointerface was synthesized into Co_3O_4/CoO spinel/rock salt nanosheets to explore this effect, where a 302 mV overpotential was observed at 10 mA·cm^{-2} [44]. DFT calculations were done to confirm multiple positive effects including improved phase transfer, the rearrangement of the

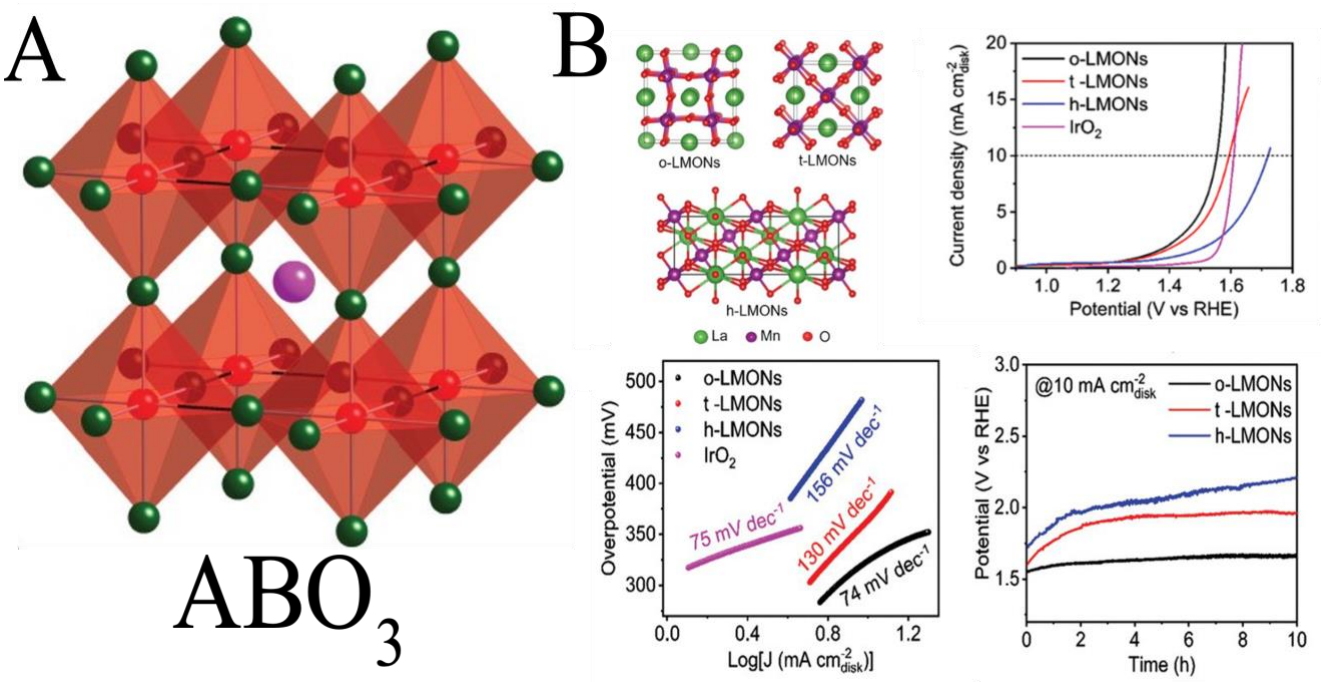

Figure 5: Perovskite Oxides for Oxygen Evolution Reaction

(A) Crystal structures for perovskite oxides. Reprinted with permission from Weller.[45] Copyright 2018 Oxford Publishing Limited.

(B) Crystal structures of LaMnO nanosheets in different crystal phases. LSV, Tafel plot, and stability test of LaMnO catalysts. Reprinted with permission from Li et al.[19] Copyright 2021 John Wiley and Sons.

electronic environment at the interface, and the presence of more active sites that all lead to the observed improvement in catalytic activity.

Interface engineering is known to be a valid strategy for improving catalyst activity thanks to its ability to increase active sites and improve intrinsic activity. The usage of close contact interfaces providing more active sites was shown in the nickel foam supported Co_3O_4 and NiFe-LDH coreshell catalyst study[43], where the improved interface not only provided more active sites for the OER but also showed increased intrinsic activity based on the ECSA of the NiFe-60/Co_3O_4@NF. With this knowledge in mind, interface engineering joins the other three previously mentioned strategies to create a robust tool set for designing better OER catalysts.

Families of Transition Metal Oxide Catalysts

Transition metal based electrocatalysts have been shown to be present in many different structures, each of which having their own unique properties and effects on their activity in the OER[45]. Examples of previously studied transition metal catalysts groups include transition metal sulfides, chalcogenides, selenides, and more[4]; in this review, we will be particularly focusing on the most common and efficient structural families of transition metal oxides, as seen in figure 4.

Transition Metal-based Perovskite Oxides

One of the most commonly explored families of transition metal oxide OER catalysts are perovskite structures. Perovskites are mixed metal oxides that consist of the general formula ABO_3 (fig. 5A), where the A site is comprised of a rare/alkaline earth metal (such as La, Sr, Ba, and Ca), while B sites are typically first row transition metals (Ni, Fe, Co, Mn, and Cr)[46]. In the case of OER activity, the elements present at the A site mainly affect the

oxygen adsorption ability of the catalyst and the B sites affect the reactivity of the adsorbed oxygens. One of the primary strengths of perovskites is the significant tunability of their structures owing to the ability of the A and B sites to be partially replaced by additional elements of different valences and sizes. Through this variance in structure, one can see the effect that unique 3D electronic structure has on OER activity.

There are many synthetic routes for producing transition metal perovskite oxides with specific parameters and nanostructures. Among these routes are wet chemical syntheses such as sol-gel, aero-gel and hydrothermal methods, solid-state synthesis, and electrodeposition/electrospinning routes. In the past, solid-state synthesis has been the most commonly employed method for producing perovskite oxides, however they have encountered issues with low surface areas as a result of high temperature calcinations. Some wet chemical routes may help remedy this problem, such as citric acid assisted sol-gel synthesis. In this route, citric acid is used as a complexation agent that will lower the temperatures required for the oxide synthesis, thus providing increasing the surface area of the final product alongside porous nanostructures[47].
While transition metal perovskite oxides have shown promising OER activity in their initial state, much work has been done to show the effectiveness of the different regulation strategies in improving perovskite OER activities. The phase engineering strategy in perovskite synthesis was exemplified through the wet chemical synthesis of $LaMnO_3$ nanosheets in orthorhombic, tetragonal, and hexagonal structures[19]. Here, $LaMnO_3$ nanosheets were produced through a salt-templated synthesis where the powder intermediates were annealed at 20-, 30-, and 50-minute intervals to produce the orthorhombic, tetragonal, and hexagonal structures respectively (crystal structures shown in fig. 5B). The OER activities of these different phase nanosheets were observed to confirm the dominance of the orthorhombic nanosheets above the other phases with a low overpotential of 324 mV at 10 $mA \cdot cm^{-2}$. The higher activity of the orthorhombic structures was attributed to e_g electron fillings closer to the ideal value of unity, increased oxygen vacancies, and improved hybridization of Mn-O covalent bonds. The impact of architecture in perovskite oxide structure was shown through a colloidal crystal template synthesis of 3D ordered microporous $LaFeO_3$[48]. This unique three-dimensional structure (3DOM) showed better OER and HER activity at 420 mV $mA \cdot cm^{-2}$ than the base $LaFeO_3$ perovskite, with the indication that the cubic structure of the 3DOM structure proved more effective than base $LaFeO_3$ orthorhombic structure as well. Additional OER improvements were displayed once a small amount of Co was doped into the 3DOM lattice with a lower overpotential of 410 mV $mA \cdot cm^{-2}$ and the lowest tafel slope 56 mV dec^{-1}. Here, the microporous structure facilitated better charge and mass transport as reactants had an easier pathway to active sites. Finally, interface engineering is displayed as an effective strategy through the sol-gel synthesis of a $LaNiO_3$/NiO heterostructure for controlled cation exsolution[49]. These heterostructures show an overpotential of 334 mV (albeit at 10 $\mu A \cdot cm^{-2}$); through operando studies done on the catalyst, it was confirmed that the boosted OER performance was a result of a promoted NiOOH layer on the interface Ni sites.

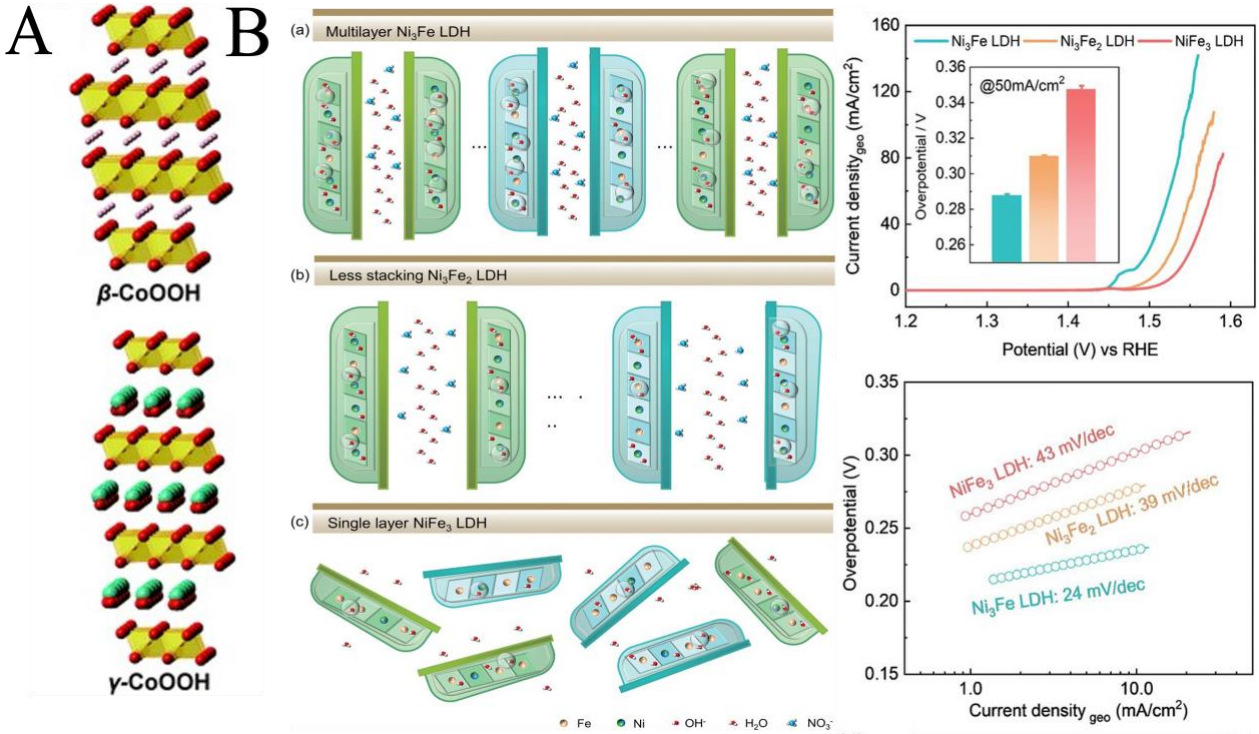

Figure 6: Layered Double Hydroxides for the Oxygen Evolution Reaction

(A) Crystal structures of Layered Double Hydroxides in different phases. Reprinted with permission from Weller.[45] Copyright 2018 Oxford Publishing Limited.

(B) Different LDH morphologies based on Ni and Fe stoichiometric ratios (left) and resulting catalytic activity (right). Reprinted with permission from Jiang et al.[52] Copyright 2022 John Wiley and Sons.

Layered Double Hydroxides

Layered Double Hydroxides (LDHs) are among some of the most outstanding candidates for OER catalysts owing to their small Tafel slopes and overpotentials. As one can see in figure 6A, LDHs are generally two-dimensional nanomaterials that are comprised of MO_6 nanosheets with anions intercalated between the nanosheet layers. These nanostructures follow the general formula of $M^{II}_{1-x}M^{III}_x(OH)_2(A^{n-})_{x/n}\cdot yH_2O$: M^{II} represents metal species in the divalent state, M^{III} represents trivalent metals, and A^{n-} represents the intercalated anions that serve to neutralize the positive charge of the metals in the nanosheets[14]. Due to the broad nature of the formula, various metals and species can be used in LDHs, thus providing the class with a high degree of flexibility in composition and structure. A myriad of synthetic routes have been demonstrated for producing LDH systems, including hydrothermal/solvothermal processes, co-precipitation, electrodeposition, and ion-exchange reactions.

By nature of being promising transition metal catalysts, extensive work has been done on LDH systems comprised of Ni, Co, and Fe with strong emphasis on binary systems of metals in the $2^+/3^+$ states. In particular, NiFe-LDH systems have been found to be some of the most active OER electrocatalyst. Computational studies over the years have attributed the OER activity of NiFe-LDHs to powerful synergy between Ni and Fe active sites present on the catalyst surface. In addition to computational studies, many experimental studies have been conducted to determine additional ways to improve LDH activity, largely through the same regulation strategies that were highlighted in the *Catalyst Activity Enhancement Strategies* section. For example, interface engineering was shown effective through the development of NiCo-LDH nanosheet/NiCoS hybrid arrays through a metal organic framework (MOF)-template surface sulfidation synthesis[50]. The heterostructure system was produced

through an initial in-situ growth process transforming commercial carbon cloth into a Co-based MOF at room temperature, followed by the production of 2D NiCo LDHs via ion exchange with nickel nitrate precursor, and finally a solvothermal process was used to induce surface sulfurization into the 3D NiCo-LDH/NiCoS structure. These sheets displayed a thickness of around 35 nm as confirmed by SEM/TEM and provided an overpotential of 207 mV at 10 mA·cm^{-2} and Tafel slope of 48 mV·dec^{-1}. Long term electrochemical studies assured the stability of the catalyst over a 24hr period, while SEM images confirmed the system's morphology remained consistent after this time. The impressive activity of this sample is attributed to electronic interactions at the interface assisting in optimizing the intermediate binding energies on the surface.

Further for NiCo-LDHs, additional metallic doping was explored through the co-precipitation synthesis of NiCoV-LDHs to show significant OER improvements[51]. Here, the NiCo-LDHs were initially prepared through co-precipitation of Ni and Co precursors, followed by addition of VCl_3 solution to the resulting powder to dope in the V. SAED and HR-TEM were used to confirm the nanocrystalline nature of the aggregated sheetlike NiCoV-LDH structures. Electrochemical analysis unveiled an overpotential of 280 mV at 10 mA·cm^{-2} and a Tafel slope of 67 mV·dec^{-1} for the NiCoV-LDH materials alongside good long-term stability and three times the TOF value of the closest performing catalyst (NiCo-LDH). XPS analysis on the materials before and after electrochemical testing was used to support the conclusion that vanadium doping increases the amount of Co^{2+} and Ni^{2+} present in the structure, thus altering the electronic structure and improving electronic interactions in the material.

The strategy of surface reconstruction also pertains to LDH structures, as seen in the synthesis of sulfur doped NiFe-LDH nanosheets through the hydrothermal method[28]. Interestingly, DFT calculations before the synthesis and XPS analysis of the products determined that the S anions substitute O inside the nanosheets rather than intercalating between nanosheet layers. These nanosheets were activated by various CV cycles before being measured for OER activity in order to induce the necessary surface reconstruction; after electrochemical activity, the S-doped NiFe-LDH sample displayed an impressive overpotential of 219 mV at 10 mA·cm^{-2} alongside an astonishing Tafel slope of 24.8 mV·dec^{-1} and stability for 360 hours. This impressive result was backed by computational calculations to confirm that the doped S changes the rate-determining step to the *OH intermediate with a lower energy barrier, thus optimizing intermediate adsorption.

Perhaps most relevant here, LDHs have also shown great susceptibility to morphological engineering, with large OER increases being reported as a result of changes to the catalyst composition. A study on the difference in OER activity between NiFe-LDHs of different compositions and crystallinities ($NiFe_3$, Ni_3Fe_2, Ni_3Fe) produced by a precipitation method was completed to illustrate the impact of morphology[52], as shown in figure 6B. In the characterization of these nanomaterials, HRTEM was used to confirm the multilayer nature of the $NiFe_3$ samples displaying high levels of crystallinity and diffraction patterns corresponding to (110) and (100) planes and lattice fringes translating to the <100> zone axis. Additionally, XAS and XANES findings indicated an increase in Fe^{3+} over Fe^{2+} species present in the Ni_3Fe samples in contrast to Ni_3Fe_2 and $NiFe_3$. Unsurprisingly, the electrochemical data then confirmed the assumed superiority of the $NiFe_3$ over its counterparts with the lowest overpotential of 287 mV (at 50 mA·cm^{-2}) and 24 mV·dec^{-1} Tafel slope; however, all three of the catalysts showed slightly increased overpotentials after 1000 cycles/400 hours. With these results, in-situ Raman work was used to investigate the different structural evolution processes occurring on the catalysts, where it was determined that the more ordered and crystalline Ni_3Fe was able to reversibly transform to the self-constructed Ni(Fe)OOH active species then back to its initial stage, while the active transformation was an irreversible process for Ni_3Fe_2 and $NiFe_3$, thus furthering knowledge of how crystallinity can affect the active phase in the OER mechanism.

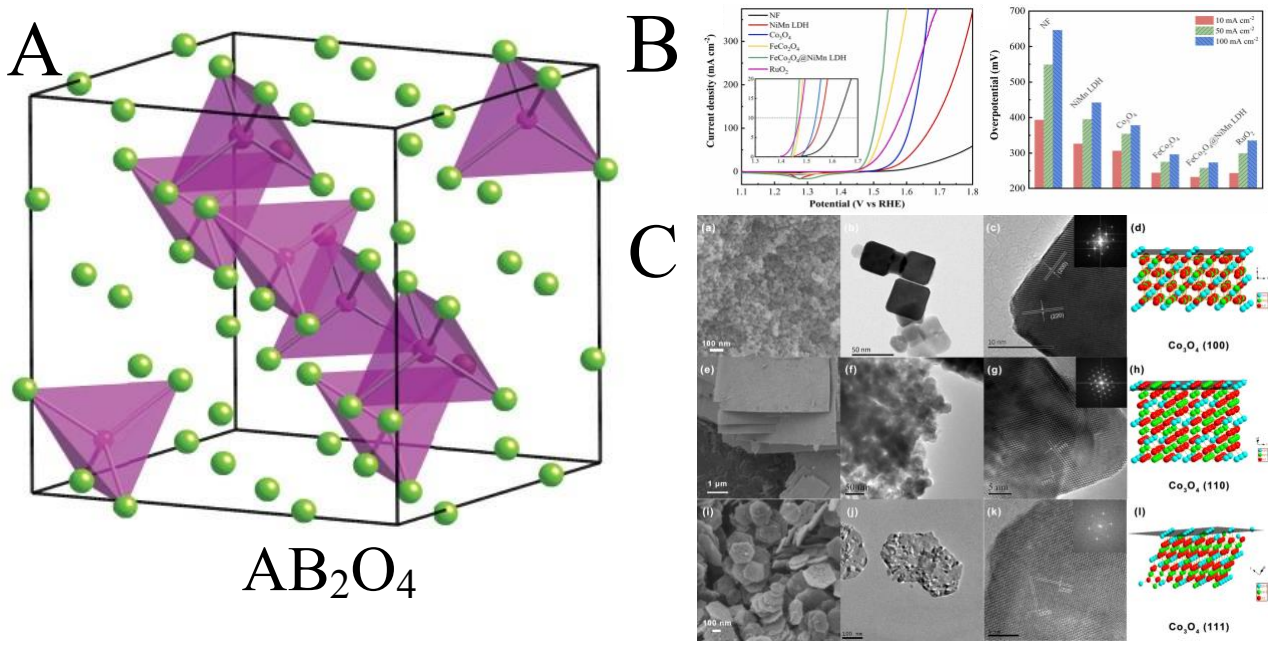

Figure 7: Spinel Oxides for the Oxygen Evolution Reaction

(A) Crystal structure of spinel oxides. Reprinted with permission from Weller.[45] Copyright 2018 Oxford Publishing Limited.

(B) Electrochemical activity of $FeCo_2O_4$@NiMn LDH nanosheets vs other observed catalysts. Reprinted with permission from Gao et al.[56] Copyright 2023 Elsevier.

(C) SEM and HRTEM of Co_3O_4 nanomaterials synthesized in different facets. Reprinted with permission from Liu et al.[60] Copyright 2018 John Wiley and Sons.

Spinel Oxides

Among the most reliable OER catalysts are the spinel family, which consists of the general formula AB_2O_4 with alternating tetrahedral and octahedral sites as displayed in figure 7A. The A^{2+} species are typically metal cations located at the tetrahedral sites, while the metal B^{3+} species reside in the octahedral sites; however, the existence of "inverse spinels" where the A^{2+} species exist at the octahedral sites and B^{3+} in the tetrahedral sites should be noted[53]. The spinel family extends to a multitude of structures including thiospinels and spinel selenides, however (in the spirit of this review) much interest has been shown in spinel oxides for the OER in past due to their relative affordability and impressive activities. Cobalt oxides such as Co_3O_4 have been extensively investigated for the OER and demonstrated some of the most impressive results among transition metal electrocatalysts. While spinel oxides have shown many advantages, important obstacles to overcome with this class of materials include limited electrical conductivity in some structures and lower stability in electrolytes. Common synthetic routes for spinel oxides include hydrothermal, solvothermal, ion exchange, etching, and coprecipitation methods.

Like the other crystalline transition metal oxide families, spinel oxides can be improved through the regulation strategies of defect engineering, morphological control, synergistic effects from interfaces, and surface reconstruction effects. The impact of defect engineering can be seen with the study of single crystalline Co_3O_4 nanosheets with deliberately introduced oxygen defects via solvothermal synthesis[54]. Here, a typical hydrothermal and annealing synthesis was done to produce initially Co_3O_4 nanosheets which were then placed into a solvothermal reaction with ethylene glycol as a reducing agent. The resulting defect-rich Co_3O_4 nanosheets were confirmed to be dominated by the [111] facet by SAED while XPS O 1s was used to confirm the increased O-vacancy. The O-rich Co_3O_4 sheets displayed an overpotential of 220 mV at 10 mA·cm^{-2} and a Tafel slope of 49.1 mV·dec^{-1}, which is a considerable improvement over the pristine Co_3O_4 nanosheets that they measured as comparison (~300 mV overpotential and ~72.3 mV·dec^{-1} Tafel slope). Finally, DFT

calculations were used to probe the difference in OER pathway with the defect structure, where it was seen that the increased oxygen vacancies further exposed Co as an active site with lower surface activation energies and narrower bandgaps displayed as a result. Another example of inducing defects can be seen in the laser ablation synthesis of V-doped $CuCo_2O_4$ nanoneedles on carbon fiber (CF) support (V-$CuCo_2O_4$/CF)[55]. Rather than formation of direct oxygen vacancies, the poorly crystalline V doped into the system also introduced a partial amorphous phase into the lattice that proved a significant improvement to the electrocatalytic activity, as shown with the 204 mV (at 100 mA·cm^{-2}), 40.7 mV·dec^{-1} and TOF of 4.02 s^{-1}. The unique laser ablation synthesis (LS) was achieved by dissolving Co, Cu, and V precursors in solution with agitated stirring, placing the pretreated CF into solution, and irradiating the solution with a KrF excimer laser; SEM, TEM, and XRD were all then used to confirm the amorphous nature of the V-doped nanoneedles in contrast to the more crystalline $CuCO_2O_4$-LS/CF control sample. DFT calculations confirmed the ability of V to protect the Co sites from deactivating via over-binding the intermediates, alongside improving surface charge distribution for surface Co close to oxygen vacancies.

As expected, powerful synergistic effects as a result of interface engineering have proven effective for improving the activity of spinel oxides as well. A 2D/2D core/shell structure of NiMn LDH nanosheets grown on $FeCo_2O_4$ spinel nanoflakes was synthesized through hydrothermal synthesis to demonstrate the strength of these synergistic effects[56]. A low overpotential of 232 mV at 10 mA·cm^{-2}, Tafel slope of 31.85 mV·dec^{-1} (fig. S1), and well-maintained 24 hour stability all confirm this effectiveness and were attributed to the increased ECSA, improved charge transport highways, and modified electronic structure of the heterostructured material. Further emphasis on synergistic effects can be seen through the hydrothermal synthesis of NiCoFeO spinel on β-$Ni(OH)_2$ nanosheet-decorated Ni foam (NF) substrate[57]. Here, lattice disorder and mixed valence/spin states induces further synergistic effects through an increased amount of metal ions in the spinel octahedral sites, thus moving the e_g orbital electron occupancy closer to unity (which is commonly agreed to be one of the most important parameters for ideal OER activity). The subsequent OER activity improvement is confirmed with an overpotential of 272 mV at 10 mA·cm^{-2} and 54 mV·dec^{-1}.

In order to understand how to utilize surface reconstruction in spinel oxides, in-situ work was done on spinel $Li_xCo_{3-x}O_4$ in different stoichiometric ratios (x=0, 0.25, 0.5, 0.75, and 1) synthesized via nitrate decomposition and heat treatment[58]. The bulk of this study was dedicated to investigating the M-O bond strength of the M_T-O-M_O backbone as the amount of lithium increases in the structure; results showed that as lithium increases, the M_T-O-M_O bond strength decreases due to lithium cations replacing cobalt at the tetrahedral sites. This subsequently increases the amount of Co_{oct}-O covalency thus improving the OER activity as confirmed by a comparative electrochemical study whereas the lithium stoichiometric ratio increases, the OER overpotential decreases. As a result, it is inferred that the increase in metal-oxygen covalency polarity between MO_4 and MO_6 (also known as the M_T-O-M_o backbone) leads to stronger surface reconstruction, thus higher OER activity. A similar study was done on $ZnCo_2O_4$ where Ni was substituted into the lattice in increasing amounts ($ZnCo_{2-x}Ni_xO_4$) where the OER activity scaled positively with the more Ni added (to a minimum overpotential of 311 mV at 25 μA·cm^{-2} and ~60 mV·dec^{-1} Tafel slope)[59]. The larger concentration of Ni further induces surface reconstruction and increases the amount of Ni^{3+} to serve as the main active site.

The favored method of morphological control has been displayed prominently in spinel oxide studies. An investigation on the impact of facet control was conducted on Co_3O_4 nanocubes, nanosheets, and nanoplates with predominantly exposed [100], [110], and [111] facets respectively[60]. These differing nanomaterials were produced through facile solvothermal and hydrothermal methods where aging and calcination times and temperatures were varied based on the targeted product. HRTEM and SAED (fig. 7C) were used to confirm sheet-like morphologies and exposed planes, where structural models were then used to display the [110] surface containing both Co^{2+} and Co^{3+} species present in contrast to [100] and [111] surfaces only containing Co^{2+}. The constructive impact of surface Co^{3+} was confirmed by electrochemical evaluation, where the [110] nanosheets outperformed the [100] nanocubes and [111] nanoplates for the OER. The increased

amount of Co^{3+} on the surface serve as additional active sites for Co^{3+} to Co^{4+} transition, thus driving the OER. Interestingly, the [100] nanocubes and [111] nanosheets show higher activity for the oxygen reduction reaction (ORR), assumedly due to the lack of surface Co^{3+}. An investigation into the influence of tetrahedral and octahedral geometries was done on $CoAl_2O_4$, $ZnCo_2O_4$, and Co_3O_4, where Co_3O_4 outperformed the other two spinel oxides due to its higher share of transition metal octahedral sites[61]. Octahedral-occupied Co corresponds to a low spin Co electronic configuration ($t_{2g}^6e_g^0$) which has considerably larger covalent overlap O p-orbitals than the high spin Co^{2+} configuration ($e^4t_2^3$). With the importance of octahedral geometry in mind, geometrical engineering through occupation of open octahedral interstices with foreign cations was done on inverse spinel $MoFe_2O_4$ nanosheets with Fe and Ni cations supported on iron foam (MNFO NS/IF)[62]. The supported nanosheets were synthesized through hydrothermal process and annealing alongside iron foam supported $NiFe_2O_4$ nanocubes (NFO NC/IF) and $MoFe_2O_4$ nanosheets (MFO NS/IF) to act as comparisons. The OER superiority of MNFO NS/IF at 250 mV at 10 $mA\cdot cm^{-2}$ and 36.9 $mV\cdot dec^{-1}$ over NFO NC/IF (269 mV, 38.2 $mV\cdot dec^{-1}$) and MFO NS/IF (300 mV, 40.6 $mV\cdot dec^{-1}$) confirmed the effectiveness of additional Fe active site exposure; additionally, Raman spectroscopy was used to confirm the occupation of Fe and Ni in the inverse spinel octahedral sites.

Amorphous Oxides

Another promising family of transition metal oxide materials are high performing amorphous oxides. While amorphous oxides may not have the uniform structures of other materials, they have shown a surprisingly efficient robustness for the OER. Some advantages of amorphous oxides include factors such as having a larger ECSA than crystalline materials, more defect structures, and increased electrolyte diffusion through the amorphous bulk matrix. Keeping in mind the importance of surface reconstruction for OER catalysts, one particular important feature of amorphous oxides is their structural flexibility aiding in reconstruction during the electrochemical process to improve catalytic activity; on the same page, amorphous materials also retain the ability to reform into more crystalline structures through reconstruction to gain further activity when required.

Similar to other transition metal oxide catalyst families reviewed, amorphous oxides can be synthesized into mixed metal oxides (binary and ternary) to boost their catalytic activity, especially when using the consistently active metal trio of Fe, Ni, and Co[63]. Fe-doped Ni and Co-based materials in particular have been shown to have increased catalytic activity when made to be amorphous, such as amorphous $NiFeO_x$/C hybrids that were sonochemically synthesized and favorably compared to crystalline FeNiO nanomaterials with OER values of 290 mV at 10 $mA\cdot cm^{-2}$ overpotential/31 $mV\cdot dec^{-1}$ Tafel slope for a-$Ni_{50}Fe_{50}O_x$/C and 297 mV at 10 $mA\cdot cm^{-2}$ overpotential/37 $mV\cdot dec^{-1}$ for $Fe_{0.1}Ni_{0.9}O$ nanocrystals[64]. Further study of amorphous FeCoNiO materials in a large range of stoichiometric ratios (a-$Fe_{100-y-z}Co_yNi_zO_x$) provided some critical mechanistic information that Fe concentrations in appropriate amounts (>40%) is crucial for lowering the Tafel slope in the amorphous system (from 73 $mV\cdot dec^{-1}$ in Fe-free systems to 40-42 $mV\cdot dec^{-1}$ in Fe-containing systems), while Co or Ni largely contribute to lowering the system's overpotential (0.38 V at 0.5 $mA\cdot cm^{-2}$ for Co/Ni-free systems for 0.23-0.27 V for Co/Ni-containing systems); an interesting observation made in this study, however, is that despite both Co and Ni being beneficial for OER activity, the a-$CoNiO_x$ system showed a worse overpotential (0.27V) than both the binary a-$FeCoO_x$ and a-$FeNiO_x$ systems (0.23-0.25V). This indicates that the degree of intermixing between Co and Ni in amorphous systems is insignificant[65,66], further reflected in figure S2. Fe dependence in Co systems was shown in a study of amorphous $Co_YFe_zO_x$ nanoflakes through a large scale $NaBH_4$ reduction synthesis at room temperature[67]. a-$Co_{2.5}Fe_{0.5}O_x$ showed the best performance of all the amorphous samples (and better than its crystalline counterpart) at

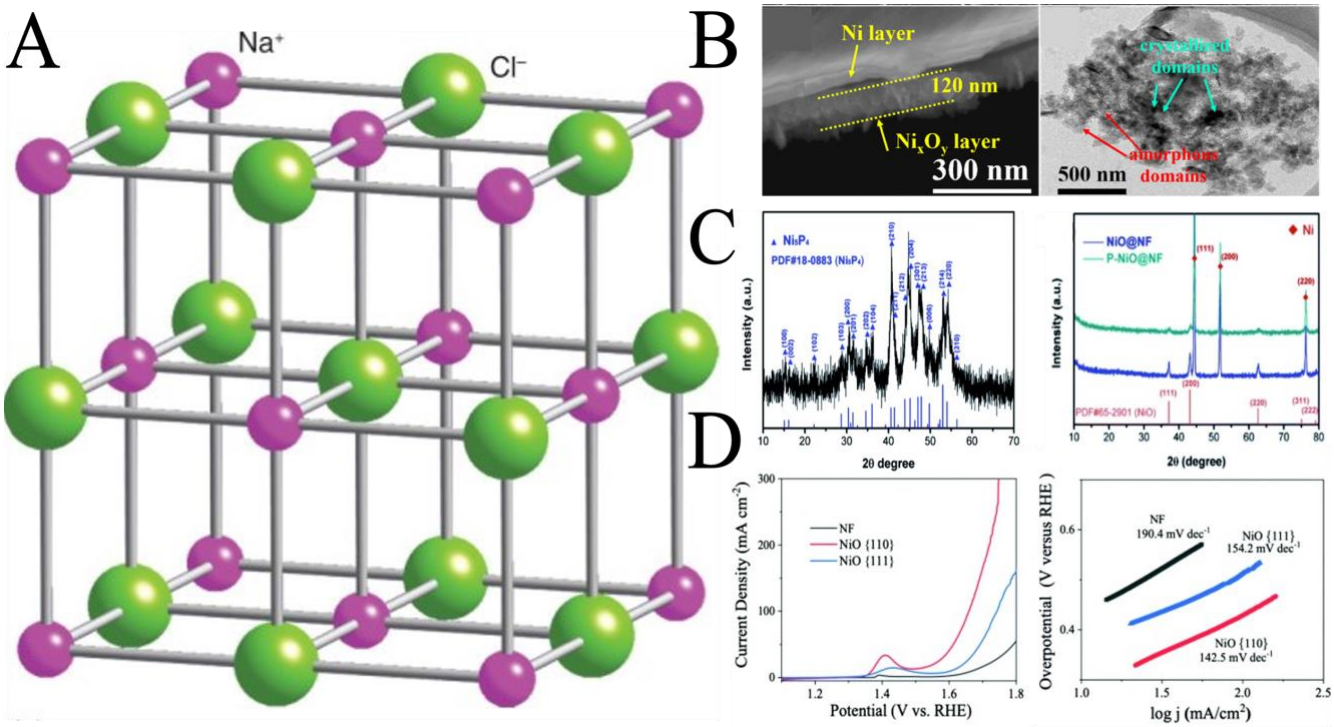

Figure 8: Rock Salt Oxides for the Oxygen Evolution Reaction

(A) Crystal structure of rock salt oxides. Reprinted with permission from Weller.[45] Copyright 2018 Oxford Publishing Limited.

(B) Oxygen defects introduced through atmospheric pressure plasma jet technique with OER analysis. SEM and HRTEM used to image different layers of sample. Reprinted with permission from Zhang et al.[70] Copyright 2021 American Chemical Society.

(C) XRD used to characterize Ni_5P_4 precursor and NiO/P-NiO catalyst post-electrochemically induced surface reconstruction. OER analysis comparing precursor, NiO, and P-NiO shown. Reprinted with permission from Dai et al.[75] Copyright 2013 Royal Society of Chemistry.

(D) Facet dependent OER activity of rock salt NiO nanomaterials. Surface reconstruction induced in situ phosphorus doping in nickel oxides for an enhanced oxygen evolution reaction. Reprinted with permission from Wang et al.[82] Copyright 2022 Royal Society of Chemistry.

280 mV at 10 mA·cm^{-2} and 39.9 mV·dec^{-1}; DFT calculations showed higher electron density for a-$Co_yFe_zO_x$ at the Fermi level than a-CoO_x alongside lowered Co site overpotential for the Fe-containing sample. These findings indicate that Fe doping aids the OER activity by optimizing the Co site electronic structure while acting as an adsorption site for the reaction intermediates. Finally, a study on the effects of amorphous nature on interfaced structures was conducted on amorphous/crystalline Ni-Fe oxide catalysts that were interfaced with Ni-Fe alloys prepared through flame synthesis[68]. Here, two catalysts were synthesized, $Ni_{0.88}Fe_{0.12}O$-1 and $Ni_{0.88}Fe_{0.12}O$-2, which were mostly amorphous and crystalline in nature respectively. The main takeaway here was that not only did the amorphous catalyst perform above the crystalline sample for the OER, but upon investigating the HER, the opposite was found with the crystalline catalyst performing better instead. Computational study proposes that this trend is due to the more ordered crystalline surface aiding in the proton study for the HER, while the disordered amorphous surface once again aids in OOH intermediate formation and thus lowers the OER activation barrier. With this observation in mind, one can understand the appeal of amorphous crystalline hybrid structures such as core-shell morphology structures comprised of an amorphous shell and crystalline core[63].

Rock Salt Metal Oxides

The last classification of transition metal oxides to be discussed in this review is the rock salt family. As shown in figure 8A, rock salt oxides are typically monometallic oxides (MO) where the metal cation and oxygen anions alternate in the face-centered cubic (fcc) lattice structure. Rock salt oxides are of particular interest in the field of OER catalysis due to their relatively large degree of tunability in their morphology and composition. For transition metal oxide rock salt electrocatalysts, Fe, Ni, and Co are commonly agreed to show the highest potential for the OER with NiO receiving the most attention. Theoretical studies have shown that NiO in different facets show varying levels of activity for the OER, with NiO(100) showing some of the most ideal activity amongst all catalysts, including PtO_2, RhO_2, and IrO_2[14]. The problem remains that while the theoretically single crystalline NiO(100) shows ideal activity, experimentally produced NiO compounds have more complicated structures and thus show higher overpotentials than desired, thus driving the search for strategies to improve NiO and other transition metal oxides to bring them to their ideal potentials.

In contrast to the more conventional perovskite and spinel oxides, rock salt oxides have not been studied as extensively for the OER, which makes them an exciting avenue to explore for potential new electrocatalyst candidates. The work that does exist examining rock salt oxide OER performance has displayed the same common improvement strategies as related metal oxide families: defect engineering, surface reconstruction, interface engineering, and most importantly for rock salt oxides, morphological control. In many of the existing studies, two or more of these strategies were used in tandem to provide even further improvement to the catalytic activity.

Defects and vacancies have been shown to play vital roles in the activity of transition metal rock salts, similar to the other transition metal oxide families. Focusing on nickel oxide systems, XPS and operando Raman spectroscopy studies were used to investigate NiO_x thin films before and after electrochemical study to investigate the effects nickel defects present in the system[69]. The NiO_x thin films were prepared through deposition method using reactive magnetron sputtering on a nickel target in argon/oxygen mixed gas, and gold disks were used for the electrode substrate. The films samples were deposited at room temperature and 600°C then had their overpotentials 10 $mA \cdot cm^{-2}$ measured initially, after 900s, and 4500s. XPS analysis of the as-prepared samples showed a sizeable peak attributed to oxygen vacancies in the O 1s spectrum, with the same peak appearing much smaller in the 600C sample. As such, the RT sample showed higher activity than its higher temperature counterpart on all trials, with an overpotential decrease from 500 mV initial to 390 mV after 4500s. To explain this difference in activity, operando Raman spectroscopy was used to display distinct differences in peaks between the two samples, where the RT sample showed two sharp peaks attributed to Ni^{III}-OOH and Ni^{III}-O that were not present in the deconvoluted 600C sample. The presence of these peaks indicates the existence of some Ni^{III} defects that provide an increase to OER activity, likely through the Ni^{II}-OH to Ni^{III}-OH transformation that occurs around 1.4V. This find was reiterated in the XPS of both samples after electrochemical analysis, where a small peak for Ni^{III}-O is present in the O 1s spectrum for the RT sample but is absent in the 600C sample. From these findings, it is concluded that the presence of nickel defects and oxygen vacancies provides benefit to OER activity. As displayed in figure 8B, a novel method for producing transition metal oxides on nickel foam (NF) support was introduced via atmospheric-pressure non-equilibrium plasma jet (APPJ) technology to prepare a nonstoichiometric nickel oxide layer directly on the NF surface in-situ at maximum thickness in as little as five minutes[70]. Samples were produced at different time intervals from one to seven minutes of plasma jet treatment, where the five minute sample (APPJ-Ni_xO_y/NF-5) showed the best catalytic activity at an overpotential of 355 mV at 10 $mA \cdot cm^{-2}$ and Tafel slope of 88 $mV \cdot dec^{-1}$. SEM imaging shows APPJ-Ni_xO_y/NF-5 as a rough surface with stacks of sheetlike materials with a layer of ~120 nm on the NF support. HRTEM confirmed the presence of amorphous and crystalline layers, where the crystalline section domain was consistent with (200) plane of cubic-phase NiO (d-spacing = 0.209 nm); the XRD patterns taken also confirm the cubic NiO structure of the crystalline domain. Finally, XPS analysis of APPJ-Ni_xO_y/NF-5 shows plentiful Ni^{3+} and Ni^{2+} peaks in the Ni 2p spectrum, and large oxygen peaks that were attributed to Ni-O and surface oxygen defects. From this information, it is inferred that the amorphous domain of the sample contains large amounts of Ni^{3+} species and oxygen defects present that then go on to enhance the OER activity.

In the first of many examples of interface engineering, rock salt NiO nanocylinders were used to form a heterostructure with spinel Co_3O_4 nanosheets in a hydrothermal synthesis that also yielded significant oxygen vacancies[71]. HRTEM confirmed the cubic crystalline nature of the NiO domains of the heterostructure with a d-spacing value of 0.208 nm corresponding to NiO (200) and a d-spacing value of 0.24 nm to confirm the Co_3O_4 spinel domains; these findings were supported by the XRD patterns for the two crystalline species being present in the heterostructure pattern. More importantly, the HRTEM image confirmed the presence of lattice distortions in the sample that is responsible for producing rich oxygen vacancies in the heterostructure. The presence of said oxygen vacancies was confirmed by via the O 1s spectrum in XPS, where three peaks corresponding to lattice oxygen, adsorbed surface oxygen, and oxygen vacancies were present. The oxygen vacancy peak for the heterostructure sample was higher than NiO and Co_3O_4. The superiority of the vacancy rich heterostructure was confirmed via electrochemical analysis, where the nanostructured hybrid showed the lowest overpotential and Tafel slope at 330 mV at 10 $mA{\cdot}cm^{-2}$ and 62.64 $mV{\cdot}dec^{-1}$ alongside 90% current retention over 10 hrs. Another study was done on Co_3O_4/NiO heterostructures, this time using heteroatom doping with P introducing additional defects into the system[72]. This heterostructure system was initially produced from synthesizing CoNi-glycerate solid spheres through simple hydrothermal synthesis followed by phosphating them with NaH_2PO_2 in a tube furnace at 400C for 2 h. Similar characterization results in XRD, TEM, and XPS to the previous Co_3O_4/NiO study were observed, indicating that the spinel and rock salt crystal structures are able to coexist and large amounts of defective oxygen reside in the system. The most impressive development here is the BET surface area of the P-containing sample compared to the bare Co_3O_4/NiO, where the P-sample has 103.70 m^2/g in surface area over the bare sample's 79.12 m^2/g. Both catalysts show a type IV isotherm, indicating a mesoporous nature that can aid in electron transport. Finally, electrochemical analysis of the catalyst displays an impressive overpotential of 283 mV at 10 $mA{\cdot}cm^{-2}$ and Tafel slope of 77 $mV{\cdot}dec^{-1}$. This compares nicely to RuO_2, which is reported to have an overpotential of 297 mV at the same current density.

One of the main difficulties that NiO faces is unfavorable adsorption properties for OH^- intermediates, thus hindering the OER mechanism. One attempt to conquer this problem was decorating NiO nanoparticles with CeO_2 and N dopants (Ce/N-NiO) to further advance electron coupling, which lead to surface electron reconfiguration[73]. The doped nanoparticles were produced through hydrothermal synthesis starting with Ni foam washed and dried with water and ethanol, followed by using Ni and Ce nitrate precursors with hexamethylenetetramine (HMT) in water to form NiO/CeO_2, then concluded with ammonia treatment to produce the Ce/N-NiO product. TEM and XRD were used to confirm a polycrystalline NiO structure present with the 0.208 nm d-spacing of the NiO (200) plane, alongside a CeO_2 crystal plane. XPS studies were done on the Ce/N-NiO sample alongside NiO, Ce-NiO, and N-NiO, where it was observed that the Ni^{3+} peak was highest in the Ce/N-NiO sample. This implied that strong electron interaction between the N-NiO and CeO_2 interface helps form more Ni^{3+} and thus improves electron transfer. Electrochemically, the Ce/N-NiO sample showed an optimal overpotential of 250 mV, which is comparable to benchmark RuO_2 at 248 mV, and favorable Tafel slope kinetics at 78 $mV{\cdot}dec^{-1}$. DFT analysis suggested that not only does Ce/N-NiO have more suitable ΔG values than its counterparts, but that electrochemical adsorption of OH^- are further optimized due to surface electronic reconstruction. A similar study involving a NiO/CeO_2 heterostructure involved synthesizing the hybrid nanowires on carbon cloth supports through hydrothermal method[74]. Here, XRD and TEM results confirmed that while NiO and CeO_2 structures were present, elements of distortion such as slightly lower d-spacing values (0.207 nm instead of 0.209) indicated a degree of lattice coupling between the two structures. Additionally, XPS study confirmed large oxygen vacancies present. Electrochemical studies at 50 $mA{\cdot}cm^{-2}$ gave the heterostructure an overpotential of 330 mV, making it comparable to commercial IrO_2@CC at 332 mV. Most notably, post electrochemical characterizations were done with XRD to confirm the presence of α-NiOOH, which was further confirmed through in-situ Raman spectroscopy showing an increase in NiOOH peaks when the voltage increased beyond 1.326 V. These findings indicated that CeO_2 influences the surface reconstruction of NiO to NiOOH, which then positively impacts OER activity. One unique and very interesting avenue of utilizing transition metal oxides comes from using transition metal catalysts outside of the

oxide family initially. Due to the inherent transformation of Ni species into oxides and oxyhydroxides in the oxygen evolution reactions, some studies have used non-oxide nickels as pre-catalysts to be reconstructed in-situ instead, such as Ni_5P_4 that also provided P doping into the resulting NiO system shown in figure 8C[75]. Ni_5P_4 pre-catalyst was first produced through ball milling method, followed by the electrode being prepared through hydrothermal synthesis. Initial XRD and TEM analyses confirmed the peak patterns of Ni_5P_4 powder for the pre-catalyst before electrochemical study. Initial voltammetry measurements for the Ni_5P_4 at 10 mA·cm^{-2} showed impressive overpotentials and Tafel slopes of 269 mV and 79.2 mV·dec^{-1}, which are respectable numbers themselves; however, CV results after 20 h of continuous OER performance demonstrated improved values of 240 mV and 53.2 mV·dec^{-1}. Post-electrochemical characterization via HRTEM confirmed the presence of NiO nanosheets, while XPS confirmed the presence of both P in the NiO nanosheets and vacancies/lattice distortions that are typically indicative of heteroatom doping. A similar study of NiO nanosheets with plentiful Ni vacancies through a non-oxide pre-catalyst was done with NiSe produced on nickel foam (NiSe@NF) formed from hydrothermal synthesis initially[76]. Similar trends in characterization were observed with the NiSe@NF electrodes before and after electrochemical analysis, however the overpotential (reported at 20 mA·cm^{-2}) was observed to be 372 mV for the initial NiSe@NF and 325 mV for Ni_xO/NiSe@NF. To further improve upon this promising technique, the proven method of iron incorporation was utilized by using 0.04M $FeCl_3$ aqueous solution as the electrolye to in-situ produce (FeNi)O/NiSe@NF. This produced an impressive overpotential of 268 mV with a 70.6 mV·dec^{-1}. XPS analyses of the samples showed that the Ni^{2+} peak in the Ni $2p_{3/2}$ spectra had a positive shift of around 0.74 eV after the incorporation of Fe, which indicates that Fe heteroatom doping does lead to structure reconstruction in Ni_xO.

Among the most common ways to improve the OER activity of rock salt metal oxides is through doping in additional transition metals into the relatively simple structure. One initial example is highly porous 3D Co-NiO nanorods produced through hydrothermal synthesis[77]. This synthesis was achieved through first using Co-doped NiC_2O_4 nanorods formed through the hydrothermal process with oxalic acid, glycerol, water, nickel, and cobalt precursors, then performing an annealing process to produce the porous NiO nanorods. Nanorods in Co concentrations from 0% to 7% were produced and characterized, where SEM imaging displayed increasing smooth, rodlike nature of the nanomaterials up to 5% Co doping, but the samples became broken and agglomerated at 6-7%. Expectedly, the electrochemical results follow the trend of increasing activity up to the optimal 5%, which showed the lowest on-set overpotential at 1.55 V versus RHE (320 mV) and an overpotential of 450 mV at 10 mA·cm^{-2}. The 5% sample also displayed the best Tafel slope kinetics at 89 mV·dec^{-1}. The decrease in activity beyond 5% indicated Co-doping is beneficial as Co incorporates into the NiO system to a certain amount without becoming destructive to the lattice. Additional transition metal doping can be taken a step further into ternary rock salt oxides, such as with FeNiCoO hollow nanospheres that were constructed alongside Ag decorations outside their shells (Ag/FNCO-HS)[78]. These samples, produced through two-step precipitation methods, were used for bifunctional OER and ORR studies, where initially a binary Ag/NCO-HS showed 310 mV overpotential. Fe was added into the first step of the precipitation process to test the effectiveness of Fe incorporation in this system, where it was found that the OER performance is higher than benchmark RuO_2. Alongside the previous consensus on Ni, Fe, and Co, for the OER, it is inferred that the Ag decorations are useful in altering heterojunction electronic structure to aid catalyst activity. Doping for rock salt oxides can extend beyond additional transition metals with heteroatom doping. A microporous N and P co-doped NiO (NP/NiO) was synthesized using non-templated hydrothermal synthesis alongside a N and O co-doped nickel phosphide (NO/NiP) for comparison[79]. Here, the NP/NiO material showed better activity with a 332 mV overpotential at 10 mA·cm^{-2}, which corresponded to the N adsorbing onto the NiO surface and creating a beneficial synergistic effect alongside increased electron transport by the P atom. The strength of synergistic effects can additionally be observed in the study in figure S3 of NiO_x film grown on spinel Co_3O_4 nanowire arrays also grown on carbon cloth support (NiO_x@Co_3O_4/CC)[80]. This sample was produced through plasma enhanced atomic layer deposition (PE-ALD). At 10 mA·cm^{-2}, the heterostructured system shows an overpotential of 360 mV and 107 mV·dec^{-1} Tafel slope, alongside impressive stability over an 11 h stability test.

One of the largest benefits to transition metal oxides is their geometrical and morphological tunability as a result of their relatively simple structure, allowing one to produce rock salt oxides possessing different facets, crystal phases, amorphous structures, and more. To start with, one can see the influence of combined crystallinities in the structure being used to increase activity through a study on cellulose-partially-reduced NiO (CL-prNiO)[81]. Produced through hydrothermal method, TEM and XRD characterizations confirms the crystalline structures of (200) for NiO and (111) fcc Ni in a hybrid alongside a disordered interface in between the two that implies the presence of defects. The defect rich CL-prNiO shows the best activity at 286 mV at 10 $mA \cdot cm^{-2}$ overpotential and 43 $mV \cdot dec^{-1}$ Tafel slope. An investigation into the structural morphology of pristine NiO in the OER was done by comparing 1D NiO nanofibers (NiO-NFBS) against more conventional 3D NiO nanoparticles (NiO-NPTs)[9]. The conventional nanoparticles were synthesized through a conventional hydrothermal method using citric acid, while the 1D nanofibers were synthesized by solution blow spinning to provide them with a hollow nature. XRD confirmed both samples contained the cubic nature of NiO, while XPS indicated a higher amount of Ni^{3+} present in the NiO-NFBs. SEM was also used to confirm the hollow nature of the nanofibers. Electrochemical analysis then favored the NiO-NFBs, which was 133 mV better than the NiO-NPTs sample at 10 $mA \cdot cm^{-2}$ (322 mV vs 455 mV). This improved activity is credited to the increased ECSA, increased mass transport, and stability of the hollow nanofiber structures.

Theoretical studies have shown that NiO in different predominant crystal planes than its most stable (111) plane have ideally higher OER activity. An investigation of this idea was done with the synthesis on NiO nanobelts with predominantly exposed (110) crystal planes produced from nickel sulfate precursor compared to traditional (111) faceted nanoplates produced with nickel nitrate precursors, shown in figure 8E[82]. HRTEM was used to compare the lattice fringes between the sample where the nanoplates showed d-spacing = 0.24 nm that is typical of (111) faceted NiO, in contrast to the fringes in the nanoplates samples 0.15 nm spacings. Increased peak height in the XPS analysis indicates that the

Catalyst	Overpotential (mV at 10 mA·cm^{-2})	Tafel Slope (mV·dec^{-1})	Classification
Orthogonal $LaMnO_3$[19]	324	74	Perovskite
3DOM $LaFe_{0.8}Co_{0.2}O_3$[46]	410	56	Perovskite
NiCo LDH/NiCoS[48]	207	48	LDH
S-NiFe LDH[26]	219	24.8	LDH
$NiFe_3$ LDH[50]	287	24	LDH
O-rich Co_3O_4[52]	220	49.1	Spinel
$FeCo_2O_4$@NiMn LDH/NF[54]	232	31.85	Spinel/LDH
Co_3O_4 (110)[58]	~300	70	Spinel
$Ni_{50}Fe_{50}O_x$/C[63]	290	41	Amorphous
APPJ-NiO/NF-5[68]	355	88	Rock Salt
(FeNi)O/NiSe@NF[74]	268	70.6	Rock Salt
NiO_x@Co_3O_4/CC[78]	360	107	Rock Salt
NiO(110)[80]	382	142.5	Rock Salt

Table 2: Comparison of catalyst OER performance in different classifications and enhancement strategies.

nanobelts structure has more surface Ni and O defect sites present to aid in OER activity. As such, the nanobelt showed an improved overpotential of 382 mV at 50 mA·cm^{-2} in contrast to 462 mV for the nanoplates. The advantages of NiO(110) seen here were further reiterated in a study of NiO thin films synthesized in (111), (100), and (110) orientations via direct current sputtering on Pt films[83]. Here upon electrochemical analysis, (110) showed most favorable Tafel slope values from low overpotentials to high overpotentials at 1.55V, which was attributed to its ability to stabilize β-Ni(OH) on its surface.

Conclusion

The debilitating effects of climate change have made it important to find sustainable energy sources for the future, with water electrolysis for hydrogen storage being one of the most promising options. While the electrocatalysts that were necessary components of water electrolyzers in the past were prohibitively expensive, transition metal based electrocatalysts that can be used in alkaline systems will allow these systems to be used on a larger scale once they reach their potential.

In order to improve the catalytic activity of transition metal based electrocatalysts, several different enhancement strategies have been developed: defect and vacancy engineering, surface reconstruction, crystal phase and facet engineering, and dopant and compositional engineering at the heterogenous interface. Each of these routes have shown positive effects and promise for improving the OER activity of the tested transition metal electrocatalysts, however each strategy also displays challenges ranging from destructive nature of the techniques involves, irreversibility, challenging thermodynamics, and energy intensive synthetic routes. For this reason, it is imperative to continue exploring ways to improve and innovate the synthetic routes used to produce highly OER active transition metal electrocatalysts.

Much work has been done exploring transition metal oxide catalysts in various structures including perovskite oxides, spinel oxides, layered double hydroxides, and amorphous oxides. Each of these extensively studied systems have shown their advantages in providing high OER activity: perovskites provide a large degree of tunability in their composition; LDHs show some of the most ideal OER activity thanks to crystallinity and layered structure; the complex structure of spinel oxides in the normal and inverse structure provides opportunity for deeper mechanism studies; and the amorphous nature of amorphous oxides improves ECSA and number of defects. In contrast, rock salt structured oxides have not received as much focus. Rock salt oxides have the potential to be useful OER catalysts due to their high variability and simplistic nature, with nickel oxide having received much attention in the past. Future work is needed in designing new nickel oxide catalysts for the OER reaction, particularly through the use of strategies such as surface reconstruction, defect engineering, interface engineering, and in the case of the potentially highly active NiO(100), morphological control.

SUPPLEMENTAL INFORMATION

Document S1. Supplemental figures from reviewed literature articles.

Figure S2. Cyclic voltammograms and contour plots of amorphous oxide systems

ACKNOWLEDGMENTS

This work was financially supported by the joint collaboration of the National Science Foundation (NSF) and the German Research Foundation (DFG) (**CBET-2139971**), alongside the NSF INTERN supplement received by Darius Hayes. The authors are grateful for the support of the Colorado School of Mines, the National Renewable Energy Laboratory (NREL), the University of Oldenburg, and the German Aerospace Center (DLR).

AUTHOR CONTRIBUTIONS

Professor Ryan Richards proposed the topic of study for the project. Bryan Pivovar and Shaun Alia provided editing and discussion for the manuscript. Darius Hayes wrote and revised the manuscript.

DECLARATION OF INTERESTS

The authors declare no competing interests.

REFERENCES

(1) Zou, X.; Zhang, Y. Noble Metal-Free Hydrogen Evolution Catalysts for Water Splitting. *Chem. Soc. Rev.* **2015**, *44* (15), 5148–5180. https://doi.org/10.1039/c4cs00448e.

(2) Xu, Y.; Ming, H. Electrocatalysis for the Oxygen Evolution Reaction: Recent Development and Future Perspectives. **2017**, *46* (2). https://doi.org/10.1039/c6cs00328a.

(3) Yu, Z. Y.; Duan, Y.; Feng, X. Y.; Yu, X.; Gao, M. R.; Yu, S. H. Clean and Affordable Hydrogen Fuel from Alkaline Water Splitting: Past, Recent Progress, and Future Prospects. *Adv. Mater.* **2021**, *33* (31), 1–35. https://doi.org/10.1002/adma.202007100.

(4) Liu, Y.; Zhou, D.; Deng, T.; He, G.; Chen, A.; Sun, X.; Yang, Y.; Miao, P. Research Progress of Oxygen Evolution Reaction Catalysts for Electrochemical Water Splitting ChemSusChem. *ChemSusChem* **2021**, *14*, 5359–5383. https://doi.org/10.1002/cssc.202101898.

(5) Dresp, S.; Strasser, P. Non-Noble Metal Oxides and Their Application as Bifunctional Catalyst in Reversible Fuel Cells and Rechargeable Air Batteries. *ChemCatChem* **2018**, *10* (18), 4162–4171. https://doi.org/10.1002/cctc.201800660.

(6) Li, D.; Park, E. J.; Zhu, W.; Shi, Q.; Zhou, Y.; Tian, H.; Lin, Y.; Serov, A.; Zulevi, B.; Baca, E. D.; Fujimoto, C.; Chung, H. T.; Kim, Y. S.

Highly Quaternized Polystyrene Ionomers for High Performance Anion Exchange Membrane Water Electrolysers. *Nat. Energy* **2020**, *5* (5), 378–385. https://doi.org/10.1038/s41560-020-0577-x.

(7) Ebbesen, S. D.; Jensen, S. H.; Hauch, A.; Mogensen, M. B. High Temperature Electrolysis in Alkaline Cells, Solid Proton Conducting Cells, and Solid Oxide Cells. *Chem. Rev.* **2014**, *114* (21), 10697–10734. https://doi.org/10.1021/cr5000865.

(8) Wei, C.; Rao, R. R.; Peng, J.; Huang, B.; Stephens, I. E. L.; Risch, M.; Xu, Z. J.; Shao-Horn, Y. Recommended Practices and Benchmark Activity for Hydrogen and Oxygen Electrocatalysis in Water Splitting and Fuel Cells. *Adv. Mater.* **2019**, *31* (31), 1–24. https://doi.org/10.1002/adma.201806296.

(9) Silva, V. D.; Simões, T. A.; Grilo, J. P. F.; Medeiros, E. S.; Macedo, D. A. Impact of the NiO Nanostructure Morphology on the Oxygen Evolution Reaction Catalysis. *J. Mater. Sci.* **2020**, *55* (15), 6648–6659. https://doi.org/10.1007/s10853-020-04481-1.

(10) Fominykh, K.; Chernev, P.; Zaharieva, I.; Sicklinger, J.; Stefanic, G.; Döblinger, M.; Müller, A.; Pokharel, A.; Böcklein, S.; Scheu, C.; Bein, T.; Fattakhova-Rohlfing, D. Iron-Doped Nickel Oxide Nanocrystals as Highly Efficient Electrocatalysts for

Alkaline Water Splitting. *ACS Nano* **2015**, *9* (5), 5180–5188. https://doi.org/10.1021/acsnano.5b00520.

(11) Cadigan, C. A.; Corpuz, A. R.; Lin, F.; Caskey, C. M.; Finch, K. B. H.; Wang, X.; Richards, R. M. Nanoscale (111) Faceted Rock-Salt Metal Oxides in Catalysis. *Catal. Sci. Technol.* **2013**, *3* (4), 900–911. https://doi.org/10.1039/c2cy20373a.

(12) Sun, T.; Wang, D.; Mirkin, M. V.; Cheng, H.; Zheng, J. C.; Richards, R. M.; Lin, F.; Xin, H. L. Direct High-Resolution Mapping of Electrocatalytic Activity of Semi-Two-Dimensional Catalysts with Single-Edge Sensitivity. *Proc. Natl. Acad. Sci. U. S. A.* **2019**, *116* (24), 11618–11623. https://doi.org/10.1073/pnas.1821091116.

(13) Zhou, B.; Gao, R.; Zou, J.-J.; Yang, H.; Zhou, B.; Gao, R.; Yang, H.; Zou, J.-J. 2202336 (1 of 26) Surface Design Strategy of Catalysts for Water Electrolysis. **2022**. https://doi.org/10.1002/smll.202202336.

(14) Man, I. C.; Su, H. Y.; Calle-Vallejo, F.; Hansen, H. A.; Martínez, J. I.; Inoglu, N. G.; Kitchin, J.; Jaramillo, T. F.; Nørskov, J. K.; Rossmeisl, J. Universality in Oxygen Evolution Electrocatalysis on Oxide Surfaces. *ChemCatChem* **2011**, *3* (7), 1159–1165. https://doi.org/10.1002/cctc.201000397.

(15) Hu, C.; Zhang, L.; Gong, J. Recent Progress Made in the Mechanism Comprehension and Design of Electrocatalysts for Alkaline

Water Splitting. *Energy Environ. Sci.* **2019**, *12* (9), 2620–2645. https://doi.org/10.1039/c9ee01202h.

(16) Medford, A. J.; Vojvodic, A.; Hummelshøj, J. S.; Voss, J.; Abild-Pedersen, F.; Studt, F.; Bligaard, T.; Nilsson, A.; Nørskov, J. K. From the Sabatier Principle to a Predictive Theory of Transition-Metal Heterogeneous Catalysis. *J. Catal.* **2015**, *328*, 36–42. https://doi.org/10.1016/j.jcat.2014.12.033.

(17) Yagi, S.; Yamada, I.; Tsukasaki, H.; Seno, A.; Murakami, M.; Fujii, H.; Chen, H.; Umezawa, N.; Abe, H.; Nishiyama, N.; Mori, S. Covalency-Reinforced Oxygen Evolution Reaction Catalyst. *Nat. Commun.* **2015**, *6* (1), 8249. https://doi.org/10.1038/ncomms9249.

(18) Kim, J. S.; Kim, B.; Kim, H.; Kang, K. Recent Progress on Multimetal Oxide Catalysts for the Oxygen Evolution Reaction. *Adv. Energy Mater.* **2018**, *8* (11). https://doi.org/10.1002/aenm.201702774.

(19) Li, Q.; Wu, J.; Wu, T.; Jin, H.; Zhang, N.; Li, J.; Liang, W.; Liu, M.; Huang, L.; Zhou, J. Phase Engineering of Atomically Thin Perovskite Oxide for Highly Active Oxygen Evolution. *Adv. Funct. Mater.* **2021**, *31* (38). https://doi.org/10.1002/adfm.202102002.

(20) Elgrishi, N.; Rountree, K. J.; McCarthy, B. D.; Rountree, E. S.; Eisenhart, T. T.; Dempsey, J. L. A Practical

Beginner's Guide to Cyclic Voltammetry. *J. Chem. Educ.* **2018**, *95* (2), 197–206. https://doi.org/10.1021/acs.jchemed.S100361.

(21) Ortiz Ortega, E.; Hosseinian, H.; Aguilar Meza, I. B.; Rodríguez Vera, A.; Rosales López, M. J.; Hosseini, S. Characterization Techniques for Electrochemical Analysis. In *Material Characterization Techniques and Applications*; Ortiz Ortega, E., Hosseinian, H., Aguilar Meza, I. B., Rosales López, M. J., Rodríguez Vera, A., Hosseini, S., Eds.; Progress in Optical Science and Photonics; Springer: Singapore, 2022; pp 195–220. https://doi.org/10.1007/978-981-16-9569-8_7.

(22) Seh, Z. W.; Kibsgaard, J.; Dickens, C. F.; Chorkendorff, I.; Nørskov, J. K.; Jaramillo, T. F. Combining Theory and Experiment in Electrocatalysis: Insights into Materials Design. *Science* **2017**, *355* (6321). https://doi.org/10.1126/science.aad4998.

(23) Zhang, Y.; Fu, Q.; Song, B.; Xu, P. Regulation Strategy of Transition Metal Oxide-Based Electrocatalysts for Enhanced Oxygen Evolution Reaction. *Acc. Mater. Res.* **2022**, *3* (10), 1088–1100. https://doi.org/10.1021/accountsmr.2c00161.

(24) Wang, Y.; Zhou, T.; Jiang, K.; Da, P.; Peng, Z.; Tang, J.; Kong, B.; Cai, W. B.; Yang, Z.; Zheng, G. Reduced Mesoporous Co3O4 Nanowires as Efficient Water Oxidation

Electrocatalysts and Supercapacitor Electrodes. *Adv. Energy Mater.* **2014**, *4* (16). https://doi.org/10.1002/aenm.201400696.

(25) Zhu, M.; Zhang, C. Laser-Synthesized Ultrafine NiO Nanoparticles with Abundant Oxygen Vacancies for Highly Efficient Oxygen Evolution. *Mater. Lett.* **2022**, *321*. https://doi.org/10.1016/j.matlet.2022.132409.

(26) Peng, L.; Yang, N.; Yang, Y.; Wang, Q.; Xie, X.; Sun-Waterhouse, D.; Shang, L.; Zhang, T.; Waterhouse, G. I. N. Atomic Cation-Vacancy Engineering of NiFe-Layered Double Hydroxides for Improved Activity and Stability towards the Oxygen Evolution Reaction. *Angew. Chem. - Int. Ed.* **2021**, *60* (46), 24612–24619. https://doi.org/10.1002/anie.202109938.

(27) Kang, Y.; Wang, S.; Hui, K. S.; Wu, S.; Dinh, D. A.; Fan, X.; Bin, F.; Chen, F.; Geng, J.; Cheong, W. C. M.; Hui, K. N. Surface Reconstruction Establishing Mott-Schottky Heterojunction and Built-in Space-Charging Effect Accelerating Oxygen Evolution Reaction. *Nano Res.* **2022**, *15* (4), 2952–2960. https://doi.org/10.1007/s12274-021-3917-7.

(28) Lei, H.; Ma, L.; Wan, Q.; Tan, S.; Yang, B.; Wang, Z.; Mai, W.; Fan, H. J. Promoting Surface Reconstruction of NiFe Layered Double Hydroxide for Enhanced Oxygen Evolution. *Adv. Energy Mater.* **2022**, *12*

(48). https://doi.org/10.1002/aenm.202202522.

(29) Duan, Y.; Yu, Z.; Hu, S.; Zheng, X.; Zhang, C.; Ding, H.; Hu, B.; Fu, Q.; Yu, Z.; Zheng, X.; Zhu, J.; Gao, M.; Yu, S. Scaled-Up Synthesis of Amorphous NiFeMo Oxides and Their Rapid Surface Reconstruction for Superior Oxygen Evolution Catalysis. *Angew. Chem.* **2019**, *131* (44), 15919–15924. https://doi.org/10.1002/ange.201909939.

(30) Xu, Q. Q.; Huo, W.; Li, S. S.; Fang, J. H.; Li, L.; Zhang, B. Y.; Zhang, F.; Zhang, Y. X.; Li, S. W. Crystal Phase Determined Fe Active Sites on Fe2O3 (γ- and α-Fe2O3) Yolk-Shell Microspheres and Their Phase Dependent Electrocatalytic Oxygen Evolution Reaction. *Appl. Surf. Sci.* **2020**, *533*. https://doi.org/10.1016/j.apsusc.2020.147368.

(31) Zou, S.; Burke, M. S.; Kast, M. G.; Fan, J.; Danilovic, N.; Boettcher, S. W. Fe (Oxy)Hydroxide Oxygen Evolution Reaction Electrocatalysis: Intrinsic Activity and the Roles of Electrical Conductivity, Substrate, and Dissolution. *Chem. Mater.* **2015**, *27* (23), 8011–8020. https://doi.org/10.1021/acs.chemmater.5b03404.

(32) Hu, J.; Li, S.; Chu, J.; Niu, S.; Wang, J.; Du, Y.; Li, Z.; Han, X.; Xu, P. Understanding the Phase-Induced Electrocatalytic Oxygen Evolution Reaction Activity on FeOOH Nanostructures. *ACS Catal.* **2019**,

10705–10711. https://doi.org/10.1021/acscatal.9b03876.

(33) Meng, Y.; Song, W.; Huang, H.; Ren, Z.; Chen, S. Y.; Suib, S. L. Structure-Property Relationship of Bifunctional MnO2 Nanostructures: Highly Efficient, Ultra-Stable Electrochemical Water Oxidation and Oxygen Reduction Reaction Catalysts Identified in Alkaline Media. *J. Am. Chem. Soc.* **2014**, *136* (32), 11452–11464. https://doi.org/10.1021/ja505186m.

(34) Xiao, C.; Lu, B. A.; Xue, P.; Tian, N.; Zhou, Z. Y.; Lin, X.; Lin, W. F.; Sun, S. G. High-Index-Facet- and High-Surface-Energy Nanocrystals of Metals and Metal Oxides as Highly Efficient Catalysts. *Joule* **2020**, *4* (12), 2562–2598. https://doi.org/10.1016/j.joule.2020.10.002.

(35) Wei, R.; Fang, M.; Dong, G.; Lan, C.; Shu, L.; Zhang, H.; Bu, X.; Ho, J. C. High-Index Faceted Porous Co3O4 Nanosheets with Oxygen Vacancies for Highly Efficient Water Oxidation. *ACS Appl. Mater. Interfaces* **2018**, *10* (8), 7079–7086. https://doi.org/10.1021/acsami.7b18208.

(36) Ouyang, J.; Pei, J.; Kuang, Q.; Xie, Z.; Zheng, L. Supersaturation-Controlled Shape Evolution of α-Fe2O3 Nanocrystals and Their Facet-Dependent Catalytic and Sensing Properties. *ACS Appl. Mater. Interfaces* **2014**, *6* (15), 12505–12514. https://doi.org/10.102

1/am502358g.
(37) Wu, H.; Yang, T.; Du, Y.; Shen, L.; Ho, G. W. Identification of Facet-Governing Reactivity in Hematite for Oxygen Evolution. *Adv. Mater.* **2018**, *30* (52). https://doi.org/10.1002/adma.201804341.
(38) Zhao, J. W.; Shi, Z. X.; Li, C. F.; Gu, L. F.; Li, G. R. Boosting the Electrocatalytic Performance of NiFe Layered Double Hydroxides for the Oxygen Evolution Reaction by Exposing the Highly Active Edge Plane (012). *Chem. Sci.* **2021**, *12* (2), 650–659. https://doi.org/10.1039/d0sc04196c.
(39) Luo, Y.; Tang, Y.; Chung, T. F.; Tai, C. L.; Chen, C. Y.; Yang, J. R.; Li, D. Y. Electron Work Function: An Indicative Parameter towards a Novel Material Design Methodology. *Sci. Rep.* **2021**, *11* (1). https://doi.org/10.1038/s41598-021-90715-4.
(40) Xu, D.; Zhang, S. N.; Chen, J. S.; Li, X. H. Design of the Synergistic Rectifying Interfaces in Mott-Schottky Catalysts. *Chem. Rev.* **2023**, *123* (1), 1–30. https://doi.org/10.1021/acs.chemrev.2c00426.
(41) Huang, J.; Han, J.; Wang, R.; Zhang, Y.; Wang, X.; Zhang, X.; Zhang, Z.; Zhang, Y.; Song, B.; Jin, S. Improving Electrocatalysts for Oxygen Evolution Using NixFe3-xO4/Ni Hybrid Nanostructures Formed by Solvothermal Synthesis. *ACS Energy Lett.* **2018**, *3* (7), 1698–1707. https://doi.org/10.1021/acsenergy

lett.8b00888.

(42) Zhang, B.; Lu, T.; Ren, Y.; Huang, L.; Pang, H.; Zhao, Q.; Tian, S.; Yang, J.; Xu, L.; Tang, Y.; Tian, X. Encapsulation of Co/Co3O4 Hetero-Nanoparticles within the Inner Tips of N-Doped Carbon Nanotubes: Engineering Mott-Schottky Nanoreactors for Efficient Bifunctional Oxygen Electrocalysis toward Flexible Zinc-Air Batteries. *Chem. Eng. J.* **2022**, *448*. https://doi.org/10.1016/j.cej.2022.137709.

(43) Lv, J.; Wang, L.; Li, R.; Zhang, K.; Zhao, D.; Li, Y.; Li, X.; Huang, X.; Wang, G. Constructing a Hetero-Interface Composed of Oxygen Vacancy-Enriched Co3O4and Crystalline-Amorphous NiFe-LDH for Oxygen Evolution Reaction. *ACS Catal.* **2021**, *11* (23), 14338–14351. https://doi.org/10.1021/acscatal.1c03960.

(44) Liu, Z.; Xiao, Z.; Luo, G.; Chen, R.; Dong, C. L.; Chen, X.; Cen, J.; Yang, H.; Wang, Y.; Su, D.; Li, Y.; Wang, S. Defects-Induced In-Plane Heterophase in Cobalt Oxide Nanosheets for Oxygen Evolution Reaction. *Small* **2019**, *15* (50). https://doi.org/10.1002/smll.201904903.

(45) Weller, M. *Inorganic Chemistry 7e*; Oxford University Press: New York, NY, 2018.

(46) Kim, D.; Oh, L. S.; Park, J. H.; Kim, H. J.; Lee, S.; Lim, E. Perovskite-Based Electrocatalysts for Oxygen Evolution Reaction in Alkaline Media: A Mini Review. *Front. Chem.* **2022**, *10*. https://doi.org/10.3389/fchem.20

22.1024865.

(47) Majid, A.; Tunney, J.; Argue, S.; Wang, D.; Post, M.; Margeson, J. Preparation of SrFeO~2.85 Perovskite Using a Citric Acid Assisted Pechini-Type Method. *J. Alloys Compd.* **2005**, *398* (1–2), 48–54. https://doi.org/10.1016/j.jallcom.2005.02.023.

(48) Dai, J.; Zhu, Y.; Zhong, Y.; Miao, J.; Lin, B.; Zhou, W.; Shao, Z. Enabling High and Stable Electrocatalytic Activity of Iron-Based Perovskite Oxides for Water Splitting by Combined Bulk Doping and Morphology Designing. *Adv. Mater. Interfaces* **2019**, *6* (1). https://doi.org/10.1002/admi.201801317.

(49) Wei, Y.; Zheng, Y.; Hu, Y.; Huang, B.; Sun, M.; Da, P.; Xi, P.; Yan, C. H. Controlling the Cation Exsolution of Perovskite to Customize Heterostructure Active Site for Oxygen Evolution Reaction. *ACS Appl. Mater. Interfaces* **2022**, *14* (22), 25638–25647. https://doi.org/10.1021/acsami.2c02861.

(50) Li, J.; Wang, L.; He, H.; Chen, Y.; Gao, Z.; Ma, N.; Wang, B.; Zheng, L.; Li, R.; Wei, Y.; Xu, J.; Xu, Y.; Cheng, B.; Yin, Z.; Ma, D. Interface Construction of NiCo LDH/NiCo S Based on the 2D Ultrathin Nanosheet towards Oxygen Evolution Reaction. *Nano Res.* **2022**, *15* (6), 4986–4995. https://doi.org/10.1007/s12274-022-4144-6.

(51) Bera, K.; Karmakar, A.; Kumaravel, S.; Sam Sankar, S.; Madhu, R.;

N Dhandapani, H.; Nagappan, S.; Kundu, S. Vanadium-Doped Nickel Cobalt Layered Double Hydroxide: A High-Performance Oxygen Evolution Reaction Electrocatalyst in Alkaline Medium. *Inorg. Chem.* **2022**, *61* (10), 4502–4512. https://doi.org/10.1021/acs.inorgchem.2c00093.

(52) Jiang, W.; Faid, A. Y.; Gomes, B. F.; Galkina, I.; Xia, L.; Lobo, C. M. S.; Desmau, M.; Borowski, P.; Hartmann, H.; Maljusch, A.; Besmehn, A.; Roth, C.; Sunde, S.; Lehnert, W.; Shviro, M. Composition-Dependent Morphology, Structure, and Catalytical Performance of Nickel–Iron Layered Double Hydroxide as Highly-Efficient and Stable Anode Catalyst in Anion Exchange Membrane Water Electrolysis. *Adv. Funct. Mater.* **2022**, *32* (38). https://doi.org/10.1002/adfm.202203520.

(53) Xu, H.; Yuan, J.; He, G.; Chen, H. Current and Future Trends for Spinel-Type Electrocatalysts in Electrocatalytic Oxygen Evolution Reaction. *Coord. Chem. Rev.* **2023**, *475*. https://doi.org/10.1016/j.ccr.2022.214869.

(54) Cai, Z.; Bi, Y.; Hu, E.; Liu, W.; Dwarica, N.; Tian, Y.; Li, X.; Kuang, Y.; Li, Y.; Yang, X. Q.; Wang, H.; Sun, X. Single-Crystalline Ultrathin Co3O4 Nanosheets with Massive Vacancy Defects for Enhanced Electrocatalysis. *Adv. Energy Mater.*

2018, *8* (3). https://doi.org/10.1002/aenm.201701694.

(55) Luo, X.; Zhang, L.; Guo, M.; Liu, Z.; Wu, D.; Zhen, D.; Liu, Y. Engineering the Structural Defects of Spinel Oxide Nanoneedles by Doping of v for a Highly Efficient Oxygen Evolution Reaction. *ACS Appl. Mater. Interfaces* **2022**. https://doi.org/10.1021/acsami.2c15524.

(56) Gao, G.; Wang, K.; Wang, X. 2D/2D Core/Shell Structure of FeCo2O4 @NiMn LDH for Efficient Oxygen Evolution Reaction. *J. Alloys Compd.* **2023**, *937*. https://doi.org/10.1016/j.jallcom.2022.168478.

(57) Upale, P.; Verma, S.; Ogale, S. B. Superior Oxygen Evolution Reaction Performance of NiCoFe Spinel Oxide Nanowires in Situ Grown on β-Ni(OH)2 Nanosheet-Decorated Ni Foam: Case Studies on Stoichiometric and off-Stoichiometric Oxides. *J. Mater. Chem. A* **2023**. https://doi.org/10.1039/d2ta08994g.

(58) Sun, Y.; Wang, J.; Xi, S.; Shen, J.; Luo, S.; Ge, J.; Sun, S.; Chen, Y.; Hanna, J. V.; Li, S.; Wang, X.; Xu, Z. J. Navigating Surface Reconstruction of Spinel Oxides for Electrochemical Water Oxidation. *Nat. Commun.* **2023**, *14* (1). https://doi.org/10.1038/s41467-023-38017-3.

(59) Duan, Y.; Sun, S.; Sun, Y.; Xi, S.; Chi, X.; Zhang, Q.; Ren, X.; Wang, J.; Ong, S. J. H.; Du, Y.; Gu, L.; Grimaud, A.; Xu, Z. J. Mastering Surface Reconstruct

ion of Metastable Spinel Oxides for Better Water Oxidation. *Adv. Mater.* **2019**, *31* (12). https://doi.org/10.1002/adma.201807898.

(60) Liu, Q.; Chen, Z.; Yan, Z.; Wang, Y.; Wang, E.; Wang, S.; Wang, S.; Sun, G. Crystal-Plane-Dependent Activity of Spinel Co3O4 Towards Water Splitting and the Oxygen Reduction Reaction. *ChemElectroChem* **2018**, *5* (7), 1080–1086. https://doi.org/10.1002/celc.201701302.

(61) Sun, S.; Sun, Y.; Zhou, Y.; Xi, S.; Ren, X.; Huang, B.; Liao, H.; Wang, L. P.; Du, Y.; Xu, Z. J. Shifting Oxygen Charge Towards Octahedral Metal: A Way to Promote Water Oxidation on Cobalt Spinel Oxides. *Angew. Chem.* **2019**, *131* (18), 6103–6108. https://doi.org/10.1002/ange.201902114.

(62) Peng, Y.; Sun, L.; Yue, X.; Huang, S. Geometrical Engineering of Spinel Oxide Solid Solution to Enhance the Oxygen Evolution Reaction. *ACS Appl. Energy Mater.* **2022**, *5* (12), 15239–15246. https://doi.org/10.1021/acsaem.2c02876.

(63) Anantharaj, S.; Noda, S. Amorphous Catalysts and Electrochemical Water Splitting: An Untold Story of Harmony. *Small* **2020**, *16* (2). https://doi.org/10.1002/smll.201905779.

(64) Li, B.; Chen, S.; Tian, J.; Gong, M.; Xu, H.; Song, L. Amorphous Nickel-Iron Oxides/Carbon Nanohybrids for an Efficient and Durable Oxygen

Evolution Reaction. *Nano Res.* **2017**, *10* (11), 3629–3637. https://doi.org/10.1007/s12274-017-1572-9.

(65) Smith, R. D. L.; Prévot, M. S.; Fagan, R. D.; Trudel, S.; Berlinguette, C. P. Water Oxidation Catalysis: Electrocatalytic Response to Metal Stoichiometry in Amorphous Metal Oxide Films Containing Iron, Cobalt, and Nickel. *J. Am. Chem. Soc.* **2013**, *135* (31), 11580–11586. https://doi.org/10.1021/ja403102j.

(66) Guo, T.; Li, L.; Wang, Z. Recent Development and Future Perspectives of Amorphous Transition Metal-Based Electrocatalysts for Oxygen Evolution Reaction. *Adv. Energy Mater.* **2022**, *12* (24). https://doi.org/10.1002/aenm.202200827.

(67) Zhang, W.; Chen, G.; Du, Y.; Zhu, S.; Zhang, J.; Liu, G.; Zhang, F.; Wang, S.; Wang, X. Large-Scale Synthesis of Fe-Doped Amorphous Cobalt Oxide Electrocatalysts at Room Temperature for the Oxygen Evolution Reaction. *ACS Appl. Energy Mater.* **2022**, *5* (3), 3129–3136. https://doi.org/10.1021/acsaem.1c03748.

(68) Shi, G.; Arata, C.; Tryk, D. A.; Tano, T.; Yamaguchi, M.; Iiyama, A.; Uchida, M.; Iida, K.; Watanabe, S.; Kakinuma, K. NiFe Alloy Integrated with Amorphous/Crystalline NiFe Oxide as an Electrocatalyst for Alkaline Hydrogen and Oxygen Evolution Reactions.

ACS Omega **2023**. https://doi.org/10.1021/acsomega.3c00322.

(69) Radinger, H.; Connor, P.; Tengeler, S.; Stark, R. W.; Jaegermann, W.; Kaiser, B. Importance of Nickel Oxide Lattice Defects for Efficient Oxygen Evolution Reaction. *Chem. Mater.* **2021**, *33* (21), 8259–8266. https://doi.org/10.1021/acs.chemmater.1c02406.

(70) Zhang, B.; Shang, X.; Jiang, Z.; Song, C.; Maiyalagan, T.; Jiang, Z. J. Atmospheric-Pressure Plasma Jet-Induced Ultrafast Construction of an Ultrathin Nonstoichiometric Nickel Oxide Layer with Mixed Ni3+/Ni2+Ions and Rich Oxygen Defects as an Efficient Electrocatalyst for Oxygen Evolution Reaction. *ACS Appl. Energy Mater.* **2021**, *4* (5), 5059–5069. https://doi.org/10.1021/acsaem.1c00623.

(71) Nam, D.; Kim, J. Development of NiO/Co3O4 Nanohybrids Catalyst with Oxygen Vacancy for Oxygen Evolution Reaction Enhancement in Alkaline Solution. *Int. J. Hydrog. Energy* **2022**, *47* (38), 16900–16907. https://doi.org/10.1016/j.ijhydene.2022.03.177.

(72) Yu, X.; Wang, X.; Wu, S.; Bai, J.; He, P.; Qin, F.; Yao, Y.; Ren, L. Insight into the Effect of P on Co3O4/NiO Heterostructure for Efficient Alkaline Oxygen Evolution Reaction. *J. Alloys Compd.* **2023**, *946*. https://doi.org/10.1016/j.jallcom.2023.169383.

(73) Yang, F.; Zhang, X.;

Zhou, L.; Lin, S.; Cao, X.; Jiang, J.; Lu, X. Tuning the Interfacial Electronic Coupling of NiO via CeO2 and Nitrogen Co-Decoration for Highly Efficient Oxygen Evolution Reaction. *Chem. Eng. J.* **2022**, *432*. https://doi.org/10.1016/j.cej.2021.134255.

(74) Yang, H.; Dai, G.; Chen, Z.; Wu, J.; Huang, H.; Liu, Y.; Shao, M.; Kang, Z. Pseudo-Periodically Coupling Ni-O Lattice with Ce-O Lattice in Ultrathin Heteronanowire Arrays for Efficient Water Oxidation. *Small* **2021**, *17* (32). https://doi.org/10.1002/smll.202101727.

(75) Dai, W.; Bai, X.; Zhu, Y. A.; Zhang, Y.; Lu, T.; Pan, Y.; Wang, J. Surface Reconstruction Inducedin Situphosphorus Doping in Nickel Oxides for an Enhanced Oxygen Evolution Reaction. *J. Mater. Chem. A* **2021**, *9* (10), 6432–6441. https://doi.org/10.1039/d0ta10925h.

(76) Dai, W.; Zhu, Y.; Ye, Y.; Pan, Y.; Lu, T.; Huang, S. Electrochemical Incorporation of Heteroatom into Surface Reconstruction Induced Ni Vacancy of NixO Nanosheet for Enhanced Water Oxidation. *J. Colloid Interface Sci.* **2022**, *608*, 3030–3039. https://doi.org/10.1016/j.jcis.2021.11.026.

(77) Cuong, N. D.; Tran, T. D.; Nguyen, Q. T.; Van Minh Hai, H.; Hoa, T. T.; Quang, D. T.; Klysubun, W.; Tran, P. D. Highly Porous Co-Doped NiO Nanorods: Facile Hydrothermal Synthesis and

Electrocatalytic Oxygen Evolution Properties. *R. Soc. Open Sci.* **2021**, *8* (9). https://doi.org/10.1098/rsos.202352.

(78) Liao, P. C.; Jhang, R. H.; Chiu, Y. H.; Valinton, J. A. A.; Yeh, C. H.; Ebajo, V. D.; Wang, C. H.; Chen, C. H. Rock Salt Oxide Hollow Spheres Achieving Durable Performance in Bifunctional Oxygen Energy Cells. *ACS Appl. Energy Mater.* **2021**, *4* (4), 3448–3459. https://doi.org/10.1021/acsaem.0c03209.

(79) Bhanja, P.; Kim, Y.; Paul, B.; Kaneti, Y. V.; Alothman, A. A.; Bhaumik, A.; Yamauchi, Y. Microporous Nickel Phosphonate Derived Heteroatom Doped Nickel Oxide and Nickel Phosphide: Efficient Electrocatalysts for Oxygen Evolution Reaction. *Chem. Eng. J.* **2021**, *405*. https://doi.org/10.1016/j.cej.2020.126803.

(80) Yang, G.; Xiang, H.; Rauf, M.; Mi, H.; Ren, X.; Zhang, P.; Li, Y. Plasma Enhanced Atomic-Layer-Deposited Nickel Oxide on Co3O4 Arrays as Highly Active Electrocatalyst for Oxygen Evolution Reaction. *J. Power Sources* **2021**, *481*. https://doi.org/10.1016/j.jpowsour.2020.228925.

(81) Yi, X.; Yin, F.; He, X.; Li, G. Partially Reduced NiO by Cellulose as a Highly Active Catalyst for Oxygen Evolution Reaction: Synergy between in Situ Generated Ni3+ and Lattice Oxygen. *Int. J. Energy Res.* **2021**, *45* (10), 15544–

15556. https://doi.org/10.1002/er.6799.

(82) Wang, J.; Xu, J.; Wang, Q.; Liu, Z.; Zhang, X.; Zhang, J.; Lei, S.; Li, Y.; Mu, J.; Yang, E.-C. NiO Nanobelts with Exposed {110} Crystal Planes as an Efficient Electrocatalyst for the Oxygen Evolution Reaction. *Phys. Chem. Chem. Phys.* **2022**, *24* (10), 6087–6092. https://doi.org/10.1039/d1cp05236e.

(83) Poulain, R.; Klein, A.; Proost, J. Electrocatalytic Properties of (100)-, (110)-, and (111)-Oriented NiO Thin Films toward the Oxygen Evolution Reaction. *J. Phys. Chem. C* **2018**, *122* (39), 22252–22263. https://doi.org/10.1021/acs.jpcc.8b05790.

(84) Zuo, S.; Wu, Z.; Zhang, G.; Chen, C.; Ren, Y.; Zheng, L.; Zhang, J.; Han, Y.; Zhang, H. Correlating Structural Disorder in Metal (Oxy)Hydroxides and Catalytic Activity in Electrocatalytic Oxygen Evolution. *Angew. Chem. Int. Ed. n/a* (n/a), e202316762. https://doi.org/10.1002/anie.202316762.

(85) Li, Y.; Bo, T.; Zuo, S.; Zhang, G.; Zhao, X.; Zhou, W.; Wu, X.; Zhao, G.; Huang, H.; Zheng, L.; Zhang, J.; Zhang, H.; Zhang, J. Reversely Trapping Isolated Atoms in High Oxidation State for Accelerating the Oxygen Evolution Reaction Kinetics. *Angew. Chem. Int. Ed.* **2023**, *62* (41), e202309341. https://doi.org/10.1002/anie.202309341.

(86) *Operando Reconstructed Molecule Fence to Stabilize NiFe-Based*

Oxygen Evolution Catalysts - Lin - 2023 - Advanced Energy Materials - Wiley Online Library. https://onlinelibrary.wiley.com/doi/full/10.1002/aenm.202300604 (accessed 2023-12-20).

(87) Wu, L.; Ning, M.; Xing, X.; Wang, Y.; Zhang, F.; Gao, G.; Song, S.; Wang, D.; Yuan, C.; Yu, L.; Bao, J.; Chen, S.; Ren, Z. Boosting Oxygen Evolution Reaction of (Fe,Ni)OOH via Defect Engineering for Anion Exchange Membrane Water Electrolysis Under Industrial Conditions. *Adv. Mater.* **2023**, *35* (44), 2306097. https://doi.org/10.1002/adma.202306097.